LAPPEENRANTA-LAHTI UNIVERSITY OF TECHNOLOGY
LUT School of Engineering Science
Chemical and Process Engineering

Master's thesis
2020

Asiia Suerbaeva

ADDITIVELY MANUFACTURED NYLON-12 ADSORBENT FOR GOLD RECOVERY

Examiners: Assoc. Prof. Eveliina Repo, D.Sc. (Tech.)
Docent Heidi Piili, D.Sc. (Tech.)

ABSTRACT

Lappeenranta-Lahti University of Technology
LUT School of Engineering Science
Chemical and Process Engineering

Asiia Suerbaeva

Additively Manufactured Nylon-12 Adsorbent for Gold Recovery

Master's Thesis

2020

66 pages, 37 figures, and 11 tables

Examiners: Assoc. Prof. Eveliina Repo, D.Sc. (Tech.)
Docent Heidi Piili, D.Sc. (Tech.)

Keywords: gold, adsorption, additive manufacturing, nylon-12, polyamide, PBF

Gold is a non-renewable metal which is widely scattered in nature. Currently, gold mining is a major gold production route, however, this industry is very expensive and causes environmental issues. Methods applied for leaching and extraction of gold from the ores include the usage of toxic compounds such as mercury (Hg) and cyanides (CN). In addition, the recovery process of gold from cyanide solution is inefficient and therefore, precious metals may be wasted in tailings. Another waste stream containing a considerable amount of gold is a waste of electric and electronic equipment. Thus, effective technology for recovery of gold from secondary sources should be created.

Additive manufacturing (AM) is a rapidly developing process due to its major advantages over conventional subtractive techniques. It provides the ability to obtain complex shapes in a short time using a wide range of materials. Freedom in design and geometries together with high accuracy allows gaining efficiency in chemical process applications. In this research, the polymer-based adsorbent was fabricated by AM, more precisely powder bed fusion (PBF) of plastic with a system of EOSINT P 395, from commercially available nylon-12. A mesh-shaped object with a layer thickness of 0.12 mm allowed achieving high surface area to enhance the adsorption process. Variety in design optimization of the adsorbent provides the ability to fulfill the requirements in different processing factories.

Adsorption of Au(III) from synthetic solution onto AM nylon-12 adsorbent was performed. The maximum adsorption capacity was achieved at pH 0 after 24h. Adsorption isotherm showed a good fitting by Langmuir equation suggesting monolayer adsorption. Kinetic data were well described by the Elovich model. According to SEM images, gold nanoparticles were formed on the polymer surface after adsorption. However, based on XPS results, majority of gold adsorbed on the polymer in the form of Au(I). Therefore, the adsorption mechanism was proposed to be chelation of Au(I) complex with nitrogen active sites.

ACKNOWLEDGEMENTS

I am deeply grateful to my thesis advisors Prof. Eveliina Repo and Docent Heidi Piili for an opportunity to be involved in very interesting research. I would like to thank them for their support, enthusiasm and valuable feedback. Special thanks to Liisa Puro, Maaret Paakkunainen and Toni Väkiparta for helping me with AAS, FTIR and SEM analyses.

I would like to offer special thanks to Samantha Kiljunen for insightful comments and discussions during my research work. My deepest appreciation goes to my office mates who literately became my second family. Without your help and encouragement, this thesis would not be materialized.

I owe my deepest gratitude to my family who supported me throughout my studies. Thank you for believing in me, for your patience and enormous love.

Asiia Suerbaeva

Lappeenranta, February, 2020

TABLE OF CONTENTS

LIST OF SYMPOLS

A_e	Elovich model parameter	mg/min g
B_e	Elovich model parameter	g/mg
C	Intraparticle diffusion constant	mg /g
C_e	Equilibrium concentration	mg /L or mg/L
C_i	Initial concentration	mg /L or mg/L
K_F	Freundlich affinity constant	L/ mg
K_L	Langmuir affinity constant	L/ mg
K_S	Sips affinity constant	L/ mg
k_1	Pseudo first order constant	1/min
k_2	Pseudo second order constant	g/ mg min
k_{dif}	Diffusion rate constant	mg /g $min^{0.5}$
n_S	Sips heterogeneity factor	-
n_F	Freundlich heterogeneity factor	-
m	Mass	g or mg
q_e	Equilibrium adsorption capacity	mg /g
q_m	Maximum adsorption capacity	mg /g
q_t	Adsorption capacity at time	mg /g
r^2	Correlation coefficient	-
T	Temperature	K or ˚C
t	Time	min
V	Volume of the solution	L or cm^3

ABBREVIATIONS

AAS	Atomic absorption spectroscopy
AM	Additive manufacturing
Au_{np}	Gold nanoparticles
BE	Binding energy
BET	Brunauer, Emmet and Teller method
BJH	Barrett-Joyner-Halenda method
EDS	Energy-dispersive X-ray spectroscopy
ERRSQ	Sum of the square of the errors
FTIR	Fourier-transform infrared spectroscopy
N12	Nylon-12
PA	Polyamide
PA12	Nylon-12
PBF	Powder bed fusion
PS1	Pseudo first order
PS2	Pseudo second order
RP	Rapid prototyping
SEM	Scanning electron microscopy
SLA	Stereolithography
SSE	Error sum of squares
XPS	X-ray photoelectron spectroscopy

1. INTRODUCTION

Additive manufacturing (AM) is a process based on manufacturing the product layer by layer using three-dimensional (3D) model data. One approach of AM was first developed by Charles Hull in 1986 known as stereolithography (SLA). After that the development in AM process resulted in different technologies such as powder bed fusion (PBF), material extrusion, inkjet printing and contour crafting. (Ngo, et al., 2018) AM allows to produce customized objects with a variety of shapes and complex geometries, using different materials with minimum material waste what makes a great advantage over conventional subtractive processes. Hence, required unique product can be manufactured in a low volume with significant time and cost reduction (Bikas, et al., 2016).

At early stage AM referred to a rapid prototyping (RP) using mainly inexpensive polymer materials during production process. Thus, AM has been widely used for prototyping by architects and designers, due to its design freedom and automation (Ngo, et al., 2018). Over the years, new developments in both manufacturing technology and variety of using materials extended dramatically the boarders of AM. Therefore, the ability to produce parts out of metals and ceramics brought AM from prototyping stage to full-on manufacturing stage. This fact significantly broad the application of AM, hence, nowadays it can be used in different industries such as construction (Bos, et al., 2016), aerospace (Kumar & Nair, 2017), medical (tissue and organ printing (Javaid & Haleem, 2019), dentistry (Miyanaji, et al., 2016), drug delivery (Zadpoor & Malda, 2017)), jewelry (Kiraz, et al., 2018), food (Lipton, et al., 2015) and commercial vehicles (Yi, et al., 2019).

Since AM has been developing rapidly over the last decades, it affected almost every kind of industries, thus chemical engineering industry is not an exception. Even though the progress in this area is still on primary level, some interesting developments have been made. For example, AM has a huge advantage over conventional manufacturing process in building micro-scale plate reactor providing high surface-area-to-volume ratios (Manoharan, et al., 2019). Périgo, et al., (2019) utilized AM technology for manufacturing of different magnets such as permanent magnets, soft magnetic materials and magnetic shape memory alloys.

Polymeric composites reinforced with carbon-fiber (van de Werken, et al., 2020), composite electrodes using eco-friendly materials instead of traditional materials for desalination (Tsai, et al., 2019), 316L stainless steel wih refined sub-granual structure for electrocatalysis (Lodhi, et al., 2019), heterogeneous geopolymer catalysts for biodiesel synthesis (Innocentini, et al., 2019) have been succsufully fabricated by AM technologies. In current work, AM was invstigaed as a tool for producing porous polymer adsorbent for metal recovery.

Gold has been included in the category of precious metals which are widely scattered in the nature and its extraction is difficult and expensive. Due to its good chemical and physical properties gold has a wide range of applications including electric and electronic devices (Antler, 1983), catalyst manufacturing (Xu, et al., 2008), jewelry (Buchtenirch, 2004) and medicine (Panyala, et al., 2009). Thus, the demand of gold is increasing whereas its concentration in the crust is extremely low (Wang, et al., 2017). Hence, the recovery of gold from secondary sources should be considered.

Currently, industries have been developing in the direction of automation of technologies. Thus, the demand in electronic devices grows rapidly. In addition, living in the era of information makes it impossible to survive without personal computers and cellphones, therefore electronic devices are an essential part of everyday life. After being discarded, electronic scrap may cause significant damages to environment due to consistency of toxic elements such as Ni, Cd, Pb, however, there are also valuables elements like Au, Ag and Pt in electronic waste (e-waste) (Fornalczyk, et al., 2013). For example, concentration of Au in one ton of cellular phone waste is about 200 g whereas in gold ore the concentration of Au is only 5-30 g per ton. (Shibata & Okuda, 2002). Therefore, electronic waste can be used as a secondary source of precious and rare metals.

Gold recovery from e-waste can be performed by various hydrometallurgical methods such as solvent extraction, chemical precipitation, membrane separations, ion exchange and adsorption (Rubcumintara, 2015). However, most of these techniques requires many steps and produce extra pollutants whereas adsorption process remains more effective due to its simplicity and low-cost. Commonly used adsorbent for gold recovery after leaching is activated carbon (Zhang, et al., 2004) however, the main disadvantage is its low selectivity.

Among different materials reported for gold adsorption it was stated that polyamides (Matsuda, et al., 1979) what makes them promising adsorbents for gold recovery from leached e-waste.

Nylon-12 is a semi-crystalline, thermoplastic polymer, which is extensively used in AM, more precisely in powder bed fusion (PBF) of plastics, due to its excellent properties and low cost. It can be used in both material extrusion and powder bed fusion, however, powder bed fusion process allows to produce more complex structure with high accuracy. Desired properties of the final product may be achieved by changing processing parameters such as laser power, scan speed and layer thickness (Flodberg, et al., 2018).

The objective of this work is to study adsorption of gold ions onto additively manufactured polymeric adsorbent. Commercially available polyamide was used as a printing material for PBF objects for gold recovery from synthetic solution. Initially, experiments were performed using nylon-12 powder to determine optimal adsorption conditions and to understand the possible binding mechanism between metal ions and polymer surface. For these purposes, the adsorption behavior of Au(III) on N12 powder at different solution pH as well as at different contact time and different initial concentrations was observed.

Additive manufactured nylon-12 adsorbent was tested by isotherm and kinetic studies at different temperatures. Several model equations were applied to describe adsorption phenomena occurred between metal ions and N12 adsorbent. Adjusting certain parameters, such as laser power and laser scanning speed during additive manufacturing process allowed to achieve more porous material. Therefore, the comparison of two AM adsorbents in terms of adsorption efficiency is presented. Regarding the environmental issues, the target was to find a possible solution for polymer reuse. Thus, fishing net produced from polyamide was used for gold recovery.

The morphologies of the adsorbent materials were characterized by certain analysis methods such as FTIR, BET, Zeta potential measurement and SEM. In addition, XPS analysis was performed for analyzing functional groups of nylon-12 before and after adsorption to understand the interaction between the adsorbent and adsorbate.

2. ADSORPTION THEORY

Adsorption is a surface phenomenon occurred at phase boundaries of two systems due to spontaneous change in the concentration of a substance at the interface. The phase where molecules of the solute are concentrated called adsorbent whereas the substance transferred from the liquid phase to the solid called adsorbate.

There are different classifications of the adsorption process. Thus, based on the interaction force that occurred between adsorbate and adsorbent adsorption may be distinguished as physical adsorption and chemisorption. Physical adsorption is defined by electrostatic attraction between substances whereas chemisorption indicates the formation of chemical bonds between molecules or atoms and adsorbent surface (Rouquerol, et al., 2014). Since chemisorption requires additional energy of activation for the formation of chemical bonds the term of activated adsorption was introduced by Taylor (1932). It is not always possible to determine exactly where it is physical adsorption or chemisorption because they can appear simultaneously or transform from one type to another (Chiou, 2002). Table 1 presents a comparison between physical and chemical adsorptions.

Table 1. Assessment of physical adsorption versus chemisorption (Repo, 2011).

	Physical adsorption	Chemisorption
Driving force	Van der Waals, hydrogen bonding, hydrophobic interactions	Chemical bonding
Heat required (kcal/mol)	5-10	10-100
Temperature range	Low temperature range	Large temperature range
Reversibility	Reversible or irreversible	irreversible
Layer formation	Monolayer or multilayer	Monolayer only

2.1 Adsorption isotherms

Adsorption isotherms are the graphical representation of the relation between the amounts of adsorbate presented in the solution at equilibrium and the amounts of compounds adsorbed on the surface of adsorbent at a constant temperature. Knowledge about adsorption equilibrium is the key information of any sorption processes. The maximum adsorption

capacity of the adsorbent reports where the adsorbent is efficient or not. (Rouquerol, et al., 2014) In addition, the shape of the isotherms gives an idea about the interaction between adsorbent and adsorbate. Giles et al., (1974) suggested four shape types of isotherms: the C-isotherm, the L-isotherm, the H-isotherm and the S-isotherm (Figure 1).

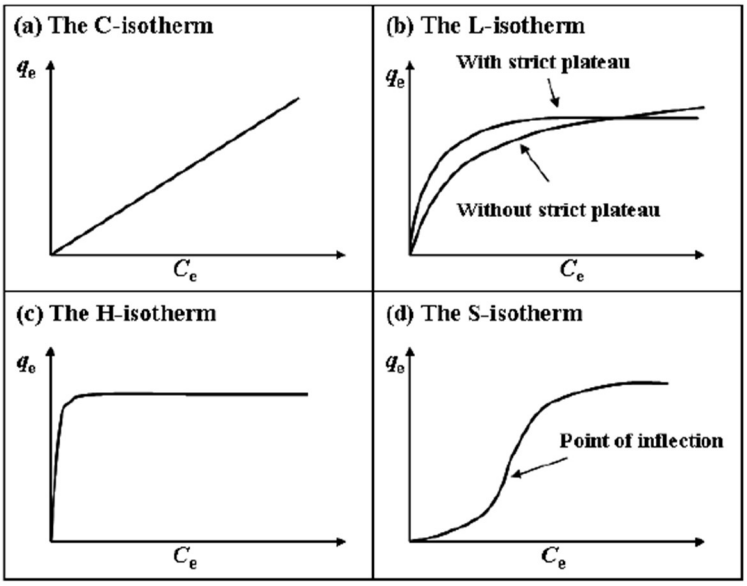

Figure 1. The main types of isotherm curves. (Repo, 2011)

The C-isotherm (Figure 1a) represents the line that passes through the origin. It means that during the adsorption process the ratio between the concentration of a substance in the solution is the same as the concentration of the solute adsorbed on the adsorbent. This ration is called the "distribution coefficient" K_d or "partition coefficient" K_p. Typically, the C-isotherms can be used only for approximation because this type of curve can be attained only at a low concentration range or at a low concentration of the substance. (Limousin, et al., 2007)

The L-isotherm (Figure 1b) refers to the process when the solid is progressively saturated. The saturation of the solid may reveal a curve with a strict plateau or without a strict plateau. The H-isotherm (Figure 1c) is the special case of L-type isotherm when the attraction between adsorbate and the solid is high so the initial slope is significant. The fourth type of isotherms is the S-isotherm (Figure 1d) which is observed occasionally. It represents the low affinity between the adsorbent and the substance at low concentrations with a subsequent increase of affinity after the point of inflection. (Repo, 2011; Limousin, et al., 2007)

Analysis of adsorption isotherms is very essential for designing adsorption processes. Currently, there are many different adsorption model isotherms which can be fitted to experimental data. Obtained model constants can provide information about surface properties of adsorbent and its interaction with an adsorbate. After modeling experimental data with model equations, linear regression analysis is applied to define the best fitting. (El-Khaiary, 2008)

2.1.1 Langmuir isotherm model

Langmuir in 1918 introduced a model for a gas-solid system that considered a limited amount of adsorption sites on the adsorbent with equal energy distribution. This model assumed the formation of adsorbate monolayer on the homogenous solid with no interactions between molecules of the adsorbate. Even though the Langmuir isotherm model was defined for the chemisorption process where covalent or ionic bonds are formed between adsorbent and adsorbate, it is often applied for different adsorption systems and can be extended for two-component adsorption process. (Liu, et al., 2019) The Langmuir model equation presented below:

$$\frac{C_e}{q_e} = \frac{1}{q_m K_L} + \frac{C_e}{q_m} \tag{2.1}$$

Where C_e is the concentration of adsorbate at equilibrium (mg/L); q_e is the amount of adsorbate at equilibrium, (mg/g); q_m is the maximum adsorption capacity (mg/g); K_L is the Langmuir constant related to the affinity of adsorbate to adsorbent (L/mg).

2.1.2 Freundlich isotherm model

The empirical equation proposed by Freundlich in 1906 describes adsorption equilibrium where heterogeneity of adsorbent is taken into account. This equation is commonly applied due to its simplicity, however, it is thermodynamically inadequate as it doesn't follow Henry's law at low concentration range. (Repo, 2011) The Freundlich isotherm equation is presented below:

$$q_e = K_F C_e^{1/n_F} \tag{2.2}$$

Where K_F is the Freundlich constant associated with the capacity of the adsorbent (mg/g); n_F is the exponent which can indicate relative energy distribution and heterogeneity of the adsorbent. If n_F value is higher than 1, the adsorption process considered favorable. The higher n_F value the higher adsorption intensity.

2.1.3 Temkin isotherm model

The Temkin isotherm, introduced by Temkin in 1940, investigates adsorption heat behavior. The heat of the adsorption diminishes linearly when the distribution of the adsorbate layer is increased. This happens because molecules of the solute presented on the surface of the solid interact with each other. The model equation may be expressed as follows (Kecili & Hussain, 2018):

$$q_e = \frac{RT}{b_T} \ln (K_T C_e) \tag{2.3}$$

Where R is an ideal gas constant (J/mol·K); T is the temperature (K); $\frac{RT}{b_T} = B_T$ (J/mg) is corresponded to the heat of adsorption; K_T is the equilibrium adsorption constant (L/mg).

2.1.4 Sips isotherm model

The Sips isotherm model is attained when the power-law expression of the Freundlich equation is imported into the Langmuir model equation. If the concentration of the adsorbate is low the Sips equation refers to Freundlich and it doesn't approach Henry's law, however, when the concentration of adsorbate is high, at high adsorbate concentration the Sips models reduce to Langmuir describing monolayer adsorption. (Hokkanen, et al., 2017) The Sips adsorption equation may be written as:

$$q_e = \frac{q_m (K_S C_e)^{n_S}}{1 + (K_S C_e)^{n_S}} \tag{2.4}$$

Where K_S is the Sips affinity constant (L/mg); n_S is the Sips isotherm exponent which related to surface heterogeneity. When n_S value is close to unity, the isotherm reduces to Langmuir

isotherm model with the homogeneous surface. In contrast, if n_S value deviates from the unity, the adsorption predicts the Freundlich model (Hokkanen, et al., 2017).

2.1.5 Toth isotherm model

Toth isotherm model is an empirical equation that is originated from the Langmuir isotherm model. The improvements were made to avoid the limitations of the Langmuir model. Therefore, the Toth isotherm can predict heterogeneous adsorption systems in both high and low ranges of the concentrations of the adsorbate. (Ayawei, et al., 2017) The equation can be given as:

$$q_e = \frac{q_m C_e}{\left(a_T + C_e^{m_T}\right)^{\frac{1}{m_T}}} \tag{2.5}$$

Where a_T is the Toth model constant (mg/L); m_T is the heterogeneity parameter.

2.2 Adsorption kinetics

Generally, there are free main stages during the adsorption process. The first stage describes the mass transmission of substance from the liquid phase to the adsorbent surface. During the second stage, internal molecular diffusion towards available adsorption sites is occurring. At the final stage, the adsorption takes place. (Kecili & Hussain, 2018) Adsorption kinetic studies help to investigate rate-controlling steps including mass transfer and possible chemical reactions occurring between solute and adsorbent as well as determine the mechanism of adsorption (Blázquez, et al., 2011).

2.2.1 Pseudo-first-order model

Lagergren introduced the empirical kinetic equation in 1898 which is extensively used for adsorption systems where the adsorption from the liquid phase has occurred. The model assumes that surface reaction between adsorbent and the solute is defined by the accessibility of active sites on the solid. Therefore, the rate of adsorption increases with increasing adsorption sites. (Fierro, et al., 2008) The PS1 model can be written as follows:

$$q_t = q_e(1 - e^{-k_1 t}) \tag{2.6}$$

Where q_t (mg/g) is the quantity of adsorbent at a time t (min); q_e is the amount of adsorbent at equilibrium (mg/g); k_1 is the first-order rate parameter (min^{-1}).

2.2.2 Pseudo-second-order model

The pseudo-second-order model equation assumes that the rate-controlling step of the sorption process is a chemical reaction. Therefore, the adsorption rate is the mater of the rate law of a second-order kinetic. It was suggested, that the accessibility of the effective sites on the surface rather than the concentration of the solute in the bulk influence the rate. (Liu, 2008) Pseudo-second-order model may be written as:

$$q_t = \frac{q_e^2 k_2 t}{1 + q_e k_2 t} \tag{2.7}$$

Where k_2 is the second-order rate parameter (g/mg·min).

2.2.3 Elovich model

The Elovich model was firstly developed by Roginsky and Zeldovich. This model can be successfully applied for chemical adsorption systems with a heterogeneous surface of the adsorbent. Elovich model is extensively used for describing adsorption of metals, dyes, and phenols on activated carbon. (Wu, et al., 2009) The model equation presented below:

$$q_t = \frac{1}{B_e} ln(1 + A_e B_e t) \tag{2.8}$$

Where A_e is the Elovich adsorption constant referred to the rate of adsorption; B_e is the Elovich model parameter related to the availability of adsorption sites.

2.2.4 Intraparticle diffusion model

Weber and Morris introduced the model in 1962 that indicates where the rate-controlling stage of the adsorption system is intraparticle diffusion. The equation of Intraparticle diffusion model presented below (Wu, et al., 2009):

$$q_t = k_{dif} t^{1/2} + C \tag{2.9}$$

Where k_{dif} is the Intraparticle diffusion rate parameter (mg/g·min$^{0.5}$); C is the constant defining the thickness of the boundary layer (mg/g·min$^{0.5}$).

3. GOLD

3.1 Properties

It is well known that gold is a transition metal, which contains unoccupied d-sublevels and therefore it occurs in several states of oxidation varying from -1 to +5 (Gimeno, 2008). However, Au(I) and Au(III) are more stable and more common forms of gold. Occupation of d-orbitals defines the number of ligands that can be coordinated along with the geometry of the complex.

Electronic configuration of Au(0) is $5d^{10}6S^1$, of Au(I) is $5d^{10}6S^0$ and of anionic Au(-1) is $5d^{10}6S^2$. This indicates that Au(I) is a stable form of gold with 10 electrons in 5d orbitals, and the possible formation of aurate anion, however, the dominance of elemental gold is unclear. (Đurovic´, et al., 2017)

Like all d^{10} elements, Au(I) forms complexes with a linear shape and the coordination number of 2 and sp-hybridization. Au(III) compounds referred to d^8 elements and forms complexes with a square-planar shape representing sp^2d-hybridization with a coordination number of 4. Usually, the formation of a square-planar complex comprises the creation of σ-bonds or π-π interactions. (Housecroft & Sharpe, 2001). The formation of complexes can be explained by Pearson's HSAB theory. According to this theory, the selectivity of the metal ions toward donor ligands can be described. Therefore, stable complexes can be formed due to the interactions between hard acids and hard bases, or soft acids and soft bases (Pearson, 1963). Au(I) refers to the ''soft" donor atom whereas Au(III) reveals transitional ''hard-soft" characteristics. The stability of the complex depends on the nature of the ligand. The stability of gold complexes with oxidation states +1 and +3 depends on the electronegativity of donor atoms of the ligand because Au(I) and Au(III) gold states refer to B-type ('soft') (Đurovic´, et al., 2017).

Among the whole transition metal group, gold is the most electronegative metal. This can be explained by the electrochemical characteristics of the gold. Since gold has the lowest value of the electrochemical potential among other metals, it is easily can be reduced to metalic gold by almost any reducing agents. Therefore, donor atoms with more electronegativity ('hard' donors) such as nitrogen, oxygen, fluorine, and chlorine can form stable complexes with Au(III). Thus, complexes of Au(III) with less electronegative donor ligands ('soft') tend to be converted into the Au(I) very easily. On the other hand, complexes that formed between Au(I) with 'hard' donor ligands can be transformed to Au(III) and Au(0). (Gimeno, 2008) The most studied Au(III) complexes are $[AuCl_4]^-$ which can be exploited for the synthesis of all other types of gold complexes (Mironov & Makotchenko, 2009). It has a square-planar shape with internal bond angles equal to 90° (Figure 2). In high

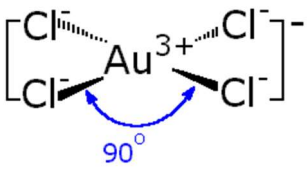

Figure 2. Square-planar shape of tetrachloride gold (III) ion. (Clarkson, 1997)

pH of the solution, hydrolysis of the chloro-gold complex occurs with subsequent formation of chloride-hydroxide complexes such as $AuCl_3OH^-$, $AuCl_2(OH)^-_2$, $AuCl(OH)^-_3$ and $Au(OH)_3$. Raising the temperature will increase the rate of hydrolysis. (Ogata & Nakano, 2005).

3.2 Gold nanoparticles

M. Faraday discovered ruby gold nanoparticles in 1857 by mixing an aqueous solution of $NaAuCl_4$ with reducing agent solution such as phosphorus in carbon disulfide. As a result, the yellow color of the sodium chloroaurate solution turned into the ruby color of the colloidal gold solution. (Thompson, 2007) The change in color can be explained by the phenomenon named surface plasmon resonance – the collective oscillation of the electrons on the surface of Au_{np} due to the interaction with light at a specific wavelength (Figure 3). When electron clouds are in resonance with the light they can absorb or scatter the light thus, different colors of colloidal gold solution appear. The properties of Au_{np} such as size, shape, surface and agglomeration state strongly affect the color of the colloidal gold solution. (Das, et al., 2011)

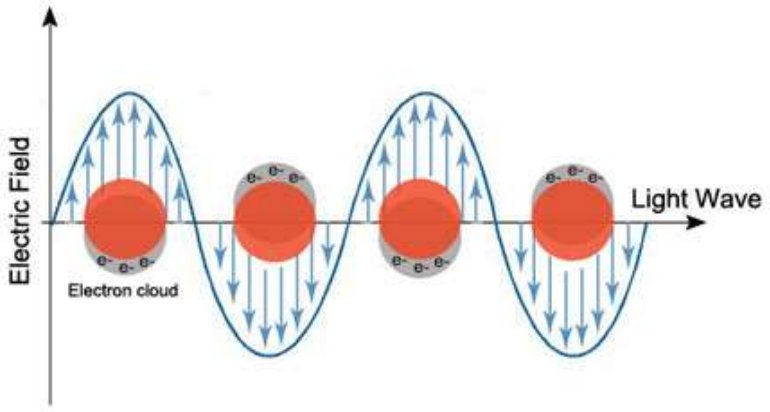

Figure 3. Surface plasmon resonance of Au_{np} with the light. (Cytodiagnostic Inc., 2017)

Based on the synthesis technique different forms of gold nanoparticles may be obtained. The common types of Au_{np} are nanospheres, nanorods, nanoshells, and nanocages. Reduction of gold from $NaAuCl_4$ solution by different reduction agents (sodium citrate, sodium borohydride) at various conditions (temperature, UV light) results in the production of gold nanospheres with a diameter range from 2nm to 100 nm. The ratio of reducing agent and amount of Au influence of the size of formed Au_{np}. (Das, et al., 2011) Figure 4 represents the influence of Au_{np} size on light absorbance at surface plasmon resonance.

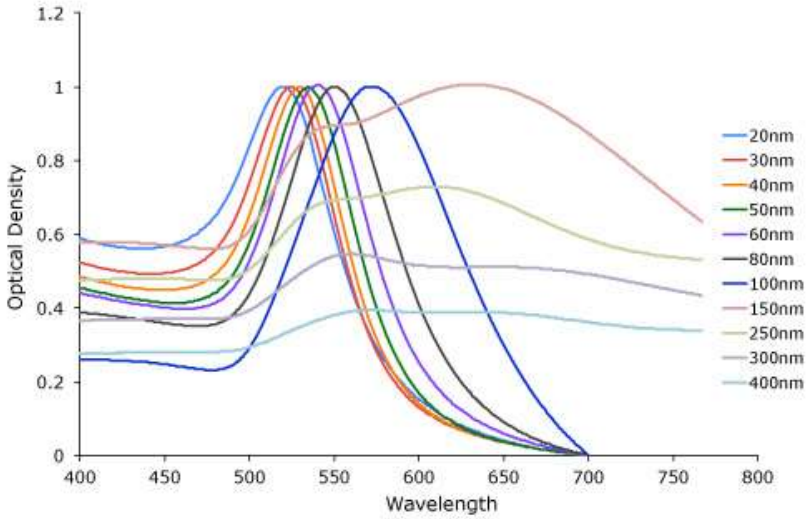

Figure 4. Dependence of Au_{np} size on surface plasmon resonance. (Cytodiagnostic Inc., 2017)

Gold nanoparticles found its application in a broad range of industries such as medicine, electronics, and catalysis, (Das et al., (2011); Pluchery et al., (2013)). Recently, the

immobilization of Au_{np} onto organic support has attracted considerable interest in catalyst application. The high electrical conductivity of gold along with chemical resistance of polymer material makes them a great alternative to conventional carbon catalyst support (Zhang, et al., 2017). In addition, the recycling of organic microsphere supports can be easily done by conventional centrifugation or filtration processes (Wen, et al., 2008). Various polymer supports for noble metals nanoparticles have been reported in the literature. For example, polystyrene microspheres were used as organic support for the deposition of Pt, Pd, and Au (Dokoutchaev, et al., 1999). Jeon et al., (2009) manufactured hierarchically structured microspheres consists of a PS-b-PEO diblock copolymer and Au_{np}. Whereas, Cheval et al., (2012) synthesized *in situ* gold nanoparticles onto the microsphere structure of nylon-6.6.

3.3 Gold recovery from secondary sources

Matsuda, et al. (1979) tested several polymers for gold recovery from diluted plating rinse, however, only nylon fibers revealed good adsorption capacity. Nylon fibers were cut in small pieces and 1 g was placed in the adsorption column so at pH 3 the amount of recovered gold was equal to 7.5g.

Yasuhito & Tomoaki (2017) also proved the selective affinity of gold ions towards polyamides. They prepared nanofiber nonwoven material from Nylon-6 and used it as an adsorbent for the synthetic solution containing Au(III), Cu(II), Al(III) and Fe(III). As a result, only gold ions were adsorbed on the Nylon-6 nanofiber nonwoven material.

Lahtinen, et al. (2017) tested different nylons for gold adsorption from electronic wastewater streams. Nylon-12 showed the highest percentage of Au(III) recovery from both synthetic solutions and leached electronic waste. AM scavenger unit was produced for gold ion uptake by continuous flow adsorption process.

Mihăilescu, et al. (2019) modified Amberlite XAD7 acrylic resin with glutamic acid thus the inert support achieved functionality by nitrogen and carboxyl groups. Au(III) recovery from waste cyanide solution was conducted at a low pH with a contact time of 60 minutes. The maximum adsorbtion capacity of the material was 14.23 mg/g. Adsorption mechanizm

was described by physical-chemical interactions between the Au(III) ions and adsorbent surface.

Liu, et al. (2019) synthesized novel bio-adsorbent based on tannic acid and dialdehyde corn starch for gold recovery from electronic waste. The adsorption capacity of the material was 298.5 mg/g at pH 2 followed by Langmuir fitting. Based on the analysis conducted after the adsorption test, it was suggested that Au(III) was adsorbed on bio-adsorbent with subsequent reduction to Au(0) due to oxidation of carbonyl groups of tannic acid.

Zhang, et al. (2015) suggested silica-gel-based polymer adsorbent grafted with dendrimer-like highly branched polymer for gold recovery from secondary sources. Adsorption tests revealed relevant adsorption capacity as well as gold selectivity in the binary solution system. Experiments were conducted at pH 2-2.5.

Liu, et al. (2020) developed crosslinked polyethyleneimine resin for adsorption of gold ions from wastewater. The high concentration of amino and hydroxyl groups on the surface provided high adsorption capacity of the material (943.5mg/g) and Au(III) selective recovery. It was convinced that gold adsorption occurred by electrostatic interaction and chelating attraction with following reduction of Au(III) to Au(0) while the OH^- groups presented on the surface were oxidized to carbonyl groups.

Gurung et al. (2011)) stated the influence of the type of amine on the gold recovery. The substitution of a diamine with tetra-amine polymer structure increases the adsorption capacity of the material almost two times. Thus, the maximum adsorption capacity attained was 1753 mg/g.

4. POLYAMIDES

4.1 Overview

Polyamides (PA) is a general name for polymer group containing amide linkage (–C(O)–NH–) within the polymer chain. Natural polyamides refer to proteins and in this case, amide linkage is called a peptide. Nylons are the biggest and oldest group of polymers in polyamide's family. They are known for their good balance of mechanical and physical properties, which build upon the density of amide linkage contained in the macromolecule chain of the polymer (Huang, et al., 2001).

The first nylon was synthesized by W. H. Carothers in 1935 by condensation polymerization of hexanediamine and adipic acid. It was called Nylon-6.6 meaning that both monomers consist of six carbon atoms (Brydson, 1999). Du Pont company started mass production of Nylon-6,6 yarn which was extensively used for brush bristles and lady's stockings due to its similar properties to natural fibers such as silk (Kim, 2000). After that, a wide range of different fiber-forming polymers was synthesized such as Nylon-6. Nylon-11, Nylon-7, Nylon-9, and others were synthesized. Nylon-12 polymer was firstly introduced by P. Lafont at Rhone-Poulenc using ω-dodecanolactam as a monomer (Griehl & Ruestem, 1970).

In the 1960s a new group of polyamides containing aromatic rings has been discovered. The co-called aramids are synthetic nylons where flexible methylene blocks are replaced by rigid benzene rings. At least 85% of amide groups should be directly attached to benzene rings (Kim, 2000). Commercially available aramid fibers such as Kevlar and Twaron found applications at military and aerospace due to their high-performance properties such as high heat resistance and excellent mechanical properties (Park & Seo, 2011).

Aliphatic nylons such as Nylon-6, 11, 12 consists of linear macromolecule chains and are thus thermoplastics. The polarity of amide linkage helps to form intermolecular hydrogen bonds between macromolecules and therefore nylons are more hydrophilic than other polymers. The density of amide groups presented in polymer defines its crystallinity. Therefore, a high concentration of amide linkage in the polymer chain means the shorter distance between –CONH– groups that indicate the increase in density, tensile strength,

rigidity, melting temperature and heat deflection temperature, hydrocarbons resistant and water absorption. (Brydson, 1999) Thus, the melting point of Nylon-6 is higher than the one of nylon-12 (Table 2). Produced aliphatic nylons are amorphous or semi-crystalline, however, the crystallinity can be increased by mechanical stretching (Kyulavska, et al., 2019).

Polyamides have been studied for many years and are among the biggest class of materials. Polyamides are remained a highly demand polymer because of their exceptional properties. Mechanical properties such as tensile strength and high impact are the most attractive properties of PA. In addition, nylons reveal electrical insulation properties, therefore, it can be used in electrical field industries. Another advantage of nylons is that the desired property can be easily obtained by adding several materials. For instance, PA composites can be synthesized by adding carbon or glass fibers. Nylons are resistant to alkaline hydrolysis and many organic solvents. In addition, some PAs show excellent barrier properties to oxygen, odor, and grease. The combination of available properties depends on the type of PA. Therefore, a variety of plastics may be produced out of polyamides. The most common fiber-forming polymers are Nylon-6 and Nylon 6,6. (Kyulavska, et al., 2019)

Table 2. Physical and thermal properties of typical polyamides (Griehl & Ruestem, 1970; Goodfellow Cambridge Limited, 2019; Greco & Nicolais, 1976).

PA	Formula	Density, g/cm^3	Melting point, °C	Tg, °C	Monomer
N6	$[–HN(CH_2)_5CO–]_n$	1.13	215-220	53	$HN–(CH_2)_5–CO$ caprolactam
N6,6	$[–OC(CH_2)_4CONH(CH_2)_6NH–]_n$	1.14	265	57	$HOOC–(CH_2)_4–COOH$ adipic acid + $H_2N–(CH_2)_6–NH_2$ hexemethylenediamine
N11	$[–HN(CH_2)_{10}CO–]_n$	1.04	184	42	$H_2N–(CH_2)_{10}–COOH$ 11-aminoundecanoic
N12	$[–HN(CH_2)_{11}CO–]_n$	1.02	178-180	41	$HN–(CH_2)_{11}–CO$ laurolactam

4.2 Synthesis

Nylons are the most extensively available petroleum-based polymers which can be manufactured by following methods: condensation of diamines and dibasic acids or condensation of diamines and dibasic acid chlorides; ring-opening polymerization of cyclic lactams, self-condensation of bifunctional amino acids, etc. PA may be classified by the position of the amine group (A) and carboxylic group (B) in the backbone. Hence, there is AABB-type of nylons such as Nylon-6,6 and AB-type such as nylon-12. In general, AABB nylons may be synthesized by direct amination of diamines and dibasic acids in the melt state. Regarding AB nylons, they can be prepared by the self-condensation of bifunctional amino acids or ring-opening polymerization of cyclic lactams in the melt state.

There are certain methods available to synthesized nylon-12. It can be obtained from ω-aminododecanoic acid, ω-aminolauric acid and lauryl lactam (Griehl & Ruestem, 1970). Below is the scheme of nylon-12 production by ring-opening polymerization from laurolactam (Figure 5).

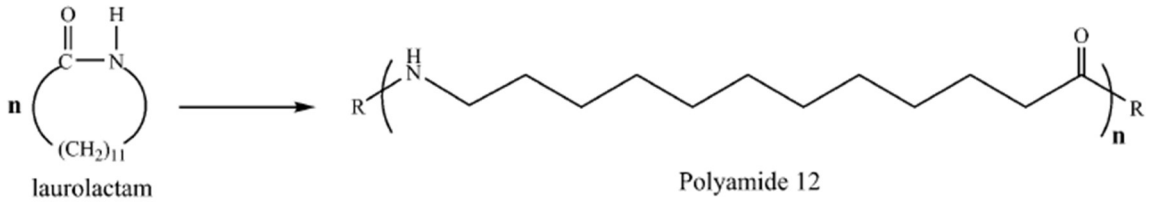

Figure 5. Ring-opening polymerization of laurolactam. (Duddleston, et al., 2016)

However, there is also an eco-friendly way to produce N12 from the bio-based monomer. In this case, nylon-12 can be obtained by a one-step fermentation of ω-aminododecanoic acid obtained from palm kernel oil. Bio-based N12 reveals similar properties as one produced by conventional methods. (Kyulavska, et al., 2019) The scheme of polycondensation of ω-aminododecanoic acid presented in Figure 6.

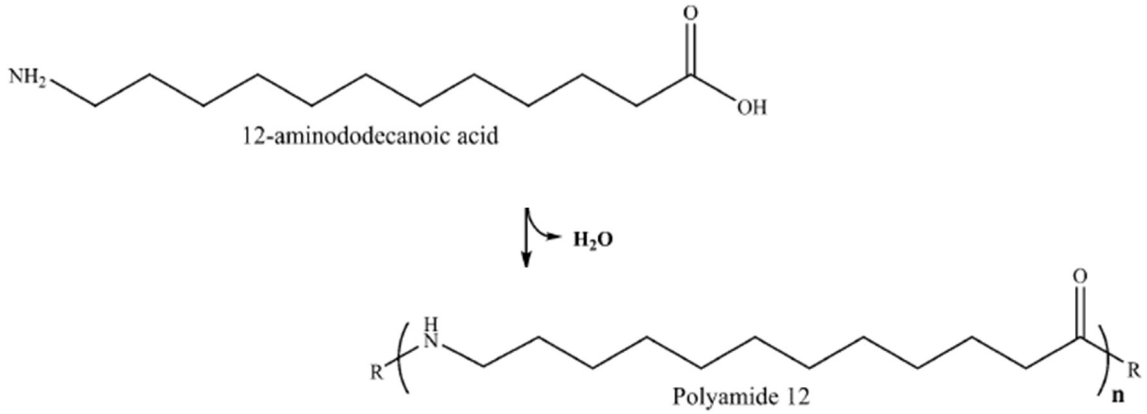

Figure 6. Production of N12 by polycondensation of 12-aminododecanoic acid. (Kyulavska, et al., 2019)

4.3 Properties and applications

PA12 contains twelfth carbon atoms in its monomer and represents a straight-chain structure. Since the density of amide linkage is lower than in nylons with fewer carbon atoms in the monomer unit, its properties are different as well. Nylon-12 has excellent resistance to chemicals, absorbs less water, as well as a good barrier to oil, grease, and oxygen. The melting point of PA12 is lower, therefore it is flexible and can be easily processed. In addition, it shows proper mechanical properties such as strength and stiffness.

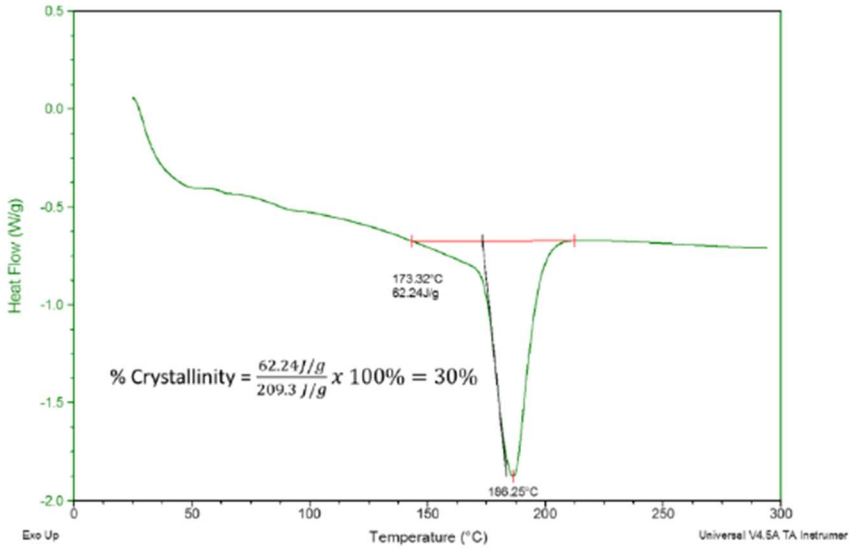

Figure 7. PA2200 powder thermogram. (Craft, 2018)

Nylon-12 has a wide range of applications. It is mostly being used as a film for lamination of cupboards in food packaging, as well as sterilized materials in pharmaceutical and medical field. Due to its electrical insulation properties, PA12 is used for cable coating in electronics. Moreover, nylon-12 can be utilized in cosmetics as well as in textile industries.

Another application for PA found in literature is gold recovery from different sidestreams. It was stated that among all metal ions existing in the solution only gold can be adsorbed on nylons therefore there is a selective affinity between gold ions and polyamides. Different types of nylon were tested, and it was shown that nylon-12 has the highest affinity towards Au(III). (Matsuda, et al., 1979; Yasuhito & Tomoaki, 2017; Lahtinen, et al., 2017).

Polyamide 12 can be utilized for additive manufacturing with both technology powder bed fusion and material extrusion. During AM process polymer undergoes mechanical and thermal impacts. For instance, during the PBF process, PA12 powder is sintered by a laser beam, and as a result, it is molded in a final product. Since polyamides are thermoplastics, it means that after applying temperature it melts whereas after cooling down polymer do not lose its properties. However, applying temperature together with some stress may cause certain changes in polymer structure such as the percentage of crystallinity. Figure 7 reveals the thermogram of PA2200 – the commercial N12 produced for PBF machines.

5. ADDITIVE MANUFACTURING

Additive manufacturing produces an object layer by layer directly from 3D CAD data without additional tooling and it may remind the digital printing, therefore, the term 3D-printing is commonly used. However, according to terminology, it is not recommended to replace these terms since the processes are different. (Gibson, et al., 2015) Nevertheless, the term 3D-printing is mostly used in literature.

The whole process of AM may be divided into several steps. At first visualization of the idea should be transformed into a 3D model using CAD software. During the design stage of the product, topology optimization should be suggested in order to achieve less material usage. After that CAD file should be converted to an STL file and only after that it can be sent to AM machine. Once the STL file has been transferred to AM machine several adjustments should be made before actual manufacturing. The position of the object to building platform as well as the necessity of additional support should be considered. Additional support is usually applied if, for example, the model has holes with a diameter of more than 6 mm to prevent overhangs. However, not all AM techniques are required support structure. After that, the AM machine set-up should be done. The next step is the building process, which is automated, however, at the beginning supervision is preferable. When manufacturing is completed, the object should be removed from the building platform and supported material may be extracted as well. After all, post-processing may be applied if needed. In general, post-processing includes abrasive methods, coating, and heat treatments. (Gibson, et al., 2015)

5.1 AM technologies

There are seven types of technologies that can be defined in AM: powder bed fusion, material extrusion, material jetting, direct energy deposition, binder jetting, sheet lamination and vat photopolymerization (Deckers, et al., 2014). Based on the technology used, the desired product can be manufactured using different materials. For example, material extrusion is implementing for prototyping, as the AM devices are commercially available at a quite low price. In this case, materials such as ABS, PLA, PET in a form of filament are commonly used. In the case of the powder bed fusion technique, the material should be in a

powder state, and metallic powder can be used as well as polymeric or ceramic powder. In this process, it is possible to obtain a very accurate object.

The material extrusion process refers to a process where the material in a form of filament applied through an extruding nozzle where it is melted and then deposited layer by layer. This process is extensively used due to its minimal initial and running cost and availability of different materials. However, this process can be used only for prototyping or consumer needs because of the visible layer lines and poor mechanical properties. (Engineering product design, 2017) Figure 8 represents the scheme of the material extrusion process

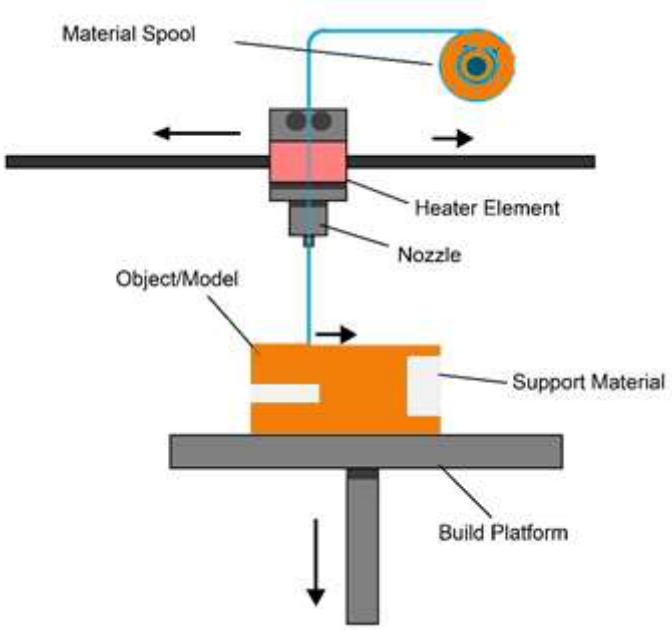

Figure 8. Material extrusion process. (Rapidsol. 3D Printing Service , 2015)

Material jetting AM process is a process where droplets of liquid build material such as photopolymer or thermoplastic material are added when exposed to a particular light wavelength. During this technique, the material is selectively jetted (much like a document printer jets ink) and then instantly cured for example by a UV lamp. The final product can be manufactured by using different materials. Materials applied in this process may vary not only in color but mechanical properties. Figure 10 shows the scheme of the material jetting process.

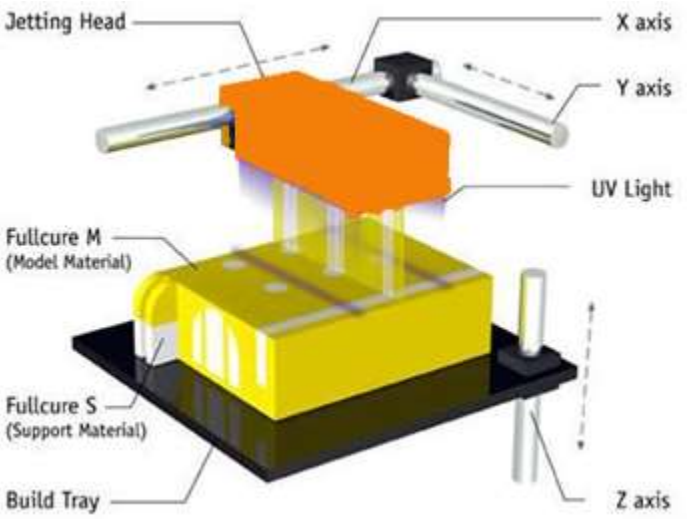

Figure 9. Material jetting process. (Rapidsol. 3D Printing Service , 2015)

Binder jetting is a method where a liquid binder agent is selectively deposited to fuse powder material into a final product. This is the only technique among others which does not use heat in order to fuse powder material. There are certain types of binders that can be applied

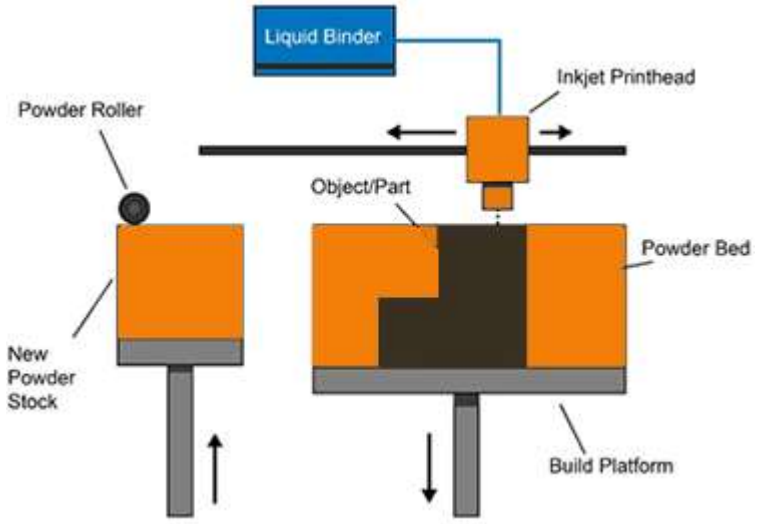

Figure 10. Binder jetting process. (Rapidsol. 3D Printing Service , 2015)

such as furan,silicates, phenolic and aqueous binders. The binder choice depends on the selected material used and customer requirements for the final product. Polymer powder, as well as ceramic and metal powder, may be used. The scheme of the binder jetting process is presented in Figure 10.

The sheet lamination process (Figure 11) is a technique where sheets of material are bonded together to build an object. Lamination can be performed by bonding, ultrasonic welding or brazing. After that laser cutting is applied to achieve a final product. Different kinds of materials can be used during a sheet lamination process such as paper, metal, plastic and woven fiber composite. Even though this process is least accurate the advantages include fast manufacturing and availability of low-cost material. However, post-processing may require more and generates more waste compared to other AM processes.

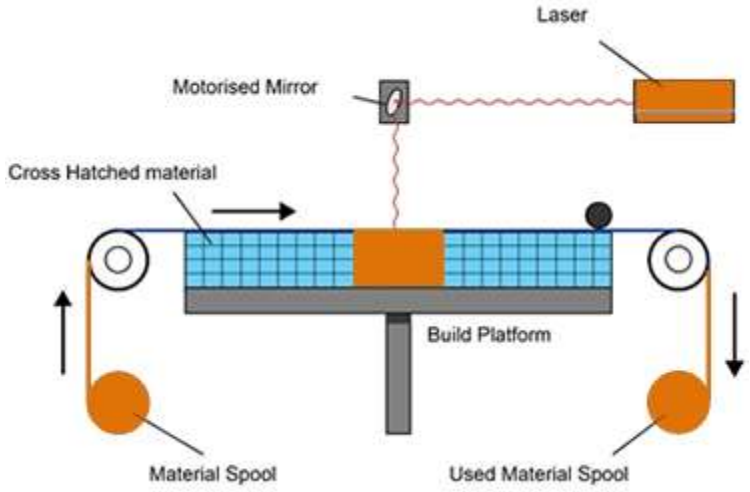

Figure 11. Sheet lamination process. (Rapidsol. 3D Printing Service , 2015)

Vat photopolymerization is a method where liquid photopolymer in a vat is selectively treated for example by ultraviolet (UV) light. The main advantage of this technique is a high resolution of the final product with a smooth surface because liquid-phase building material is exploited. The viscosity of photopolymer resin plays an essential role in the process because the deposition of a new layer is the main time-consuming step. This process can be applied in medical modeling therefore 3D models of different anatomic parts can be created based on the data from computer scans. Figure 12 reveals the scheme of the vat polymerization process.

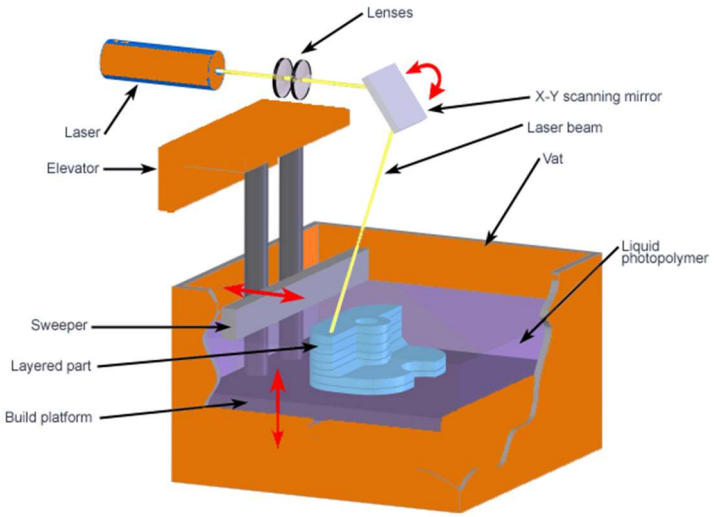

Figure 12. Vat polymerization process. (Rapidsol. 3D Printing Service , 2015)

Direct energy deposition (DED) is a process where focused thermal energy such as laser, electron beam, or plasma arc melt the material to form an object. Generally, DED uses metal in the form of either wire or powder. However, DED technology is also capable of using polymers and ceramics. During the DED process minimum of material waste is produced. There are a lot of industrial applications for this process. Thus, DED technology can be utilized in aerospace, oil&gas and marine industries due to the ability to build large and complex shapes. However, the building resolution is quite low, and the process requires high capital costs. Figure 13 exhibits a wire-based direct energy deposition process.

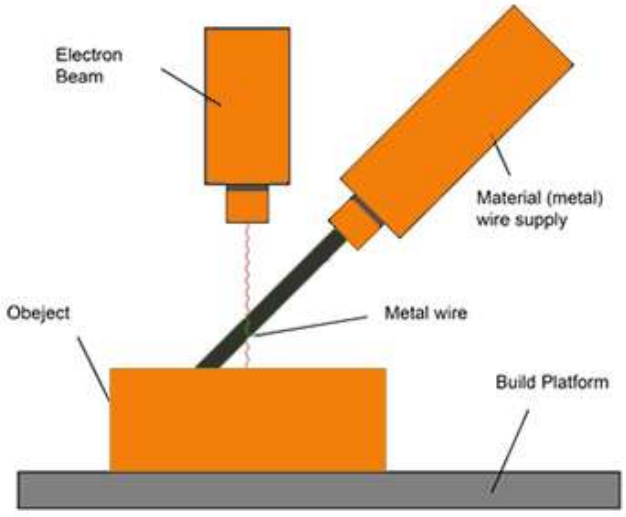

Figure 13. Wire-based direct energy deposition process. (Rapidsol. 3D Printing Service , 2015)

Powder bed fusion process (Figure 14) is a process where thermal energy provided from a laser or electron beam fuses the powder particles layer by layer forming the desired object. This technique may use any powder materials. Based on the grain size of the powder the finishing of the final product may be needed. The main disadvantage of this process is the amount of material waste.

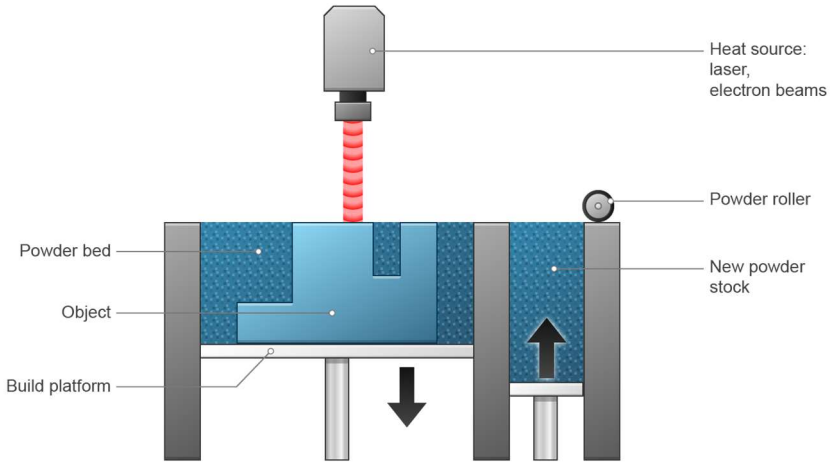

Figure 14. Powder bed fusion process. (3DEXPERIENCE Marketplace, 2018)

5.2 Powder bed fusion of plastics

Powder bed fusion (PBF) of plastics is the most promising and well-established AM technique. It founds its application as a prototyping technique as well as a small-scale manufacturing technique (Beard, et al., 2011). Typical PBF machine (Figure 13) consists of a mobile building platform, CO_2 laser source, powder roller, and powder delivery system. The main principle can be described as follows: a tank with polymer powder is being pre-heated to a temperature close to the melting point of a polymer, then powder roller spreads the first layer of powder material with chosen layer thickness on a building platform. After that, a CO_2 laser beam scans the building platform and selectively sinter the polymer powder therefore a cross-section of the building object is created. When the whole cross-section is scanned, the building platform moves one layer down whereas the tank with fresh powder moves up so the powder roller spreads a new layer of polymer. The steps are repeated until the final product is manufactured. After all, the object is removed from the powder bed. Since unsintered powder remains in the building platform, no supporting structures are needed. Powder from building platform can be reused for the next process when mixed with a fresh one in relation to 1:1. (Redwood, et al., 2017)

There is a range of parameters during the PBF process which can affect the properties of the final product. Material parameters such as powder grain size and shape, the molecular weight of the polymer and its crystallinity have a direct influence on the mechanical properties of the obtained product. Crystallinity and molecular weight of the polymer affect the tensile strength and elongation at break whereas powder size distribution influence the fusion of the powder (Hofland, et al., 2017).

Machine parameters such as energy density, layer thickness, laser scanning speed, laser power, and laser spot size change the PBF process thereby the properties of the final object also changes. Applying higher laser energy density improves the fusion of powder and affects the molecular structure of the polymer, however extremely high energy density leads to polymer destruction. This resulted to increase in tensile strength and elongation at break (Ho, et al., 1999). Layer thickness and scan spacing are the most important parameters during the process. They affect the anisotropy of the PBF manufactured part, internal structure and surface finish (Hofland, et al., 2017). Laser scanning speed and laser power influence the fusion of powder particles. If any of this parameter is too high or too low, it will lead to incomplete melting of powder particles and formation of pores with a diameter of >100 μm (Caulfield, et al., 2007). Flodberg et al., (2018) suggested that the ability to light absorption of the material together with thermal conductivity influence the porosity of final parts thus manufactured PA12 revealed porosity of 4.7%.

The most commonly used material for the PBF process is polyamide 12 (PA12) due to its availability and mechanical properties of the final products To achieve better mechanical properties or heat resistance, nylon powder can be mixed with other materials such as glass, carbon or aluminum before sintering. As was mentioned before, the PBF process allows mixing 50% of unsintered powder with a fresh one without significant loss in mechanical properties. In addition, there is another possibility to minimize polymer waste. The unsintered powder can be transformed into filaments by a single-screw extruder thus the filaments can be used in the material extrusion process (Feng, et al., 2019).

6. MATERIALS AND METHODS

6.1 Materials and chemicals

Polymer powder was provided by EOS GmbH, Germany and has been utilized for both batch adsorption experiments and the manufacturing of AM objects. Commercial PA2200 is a fine-powder with mean grain size 50 μm which reveals higher crystallinity and higher melting point than usual polyamides. Properties of N12 powder are presented in table 3.

Table 3. PA2200 powder properties. (EOS GmbH - Electro Optical System, 2017)

Bulk density, g/cm^3	Melting temperature, C°	Crystallization temperature, C°	Molecular weight	
			Mol mean M_n, g/mol	Weight mean M_w, g/mol
>0.430	184	138	15000	29000

Gold spectroscopy standard solution (1000ppm) was purchased from Sigma-Aldrich Co. LLC (Finland) and used for the preparation of the synthetic solution. Hydrochloric acid (≥37%) and sodium hydroxide were used for preparation 1M, 0.1M solutions for pH adjustment. High-purity deionized water of 15 MΩ cm resistivity produced by CENTRA-R 60/120 system provided by Elga purification system (Veolia Water, UK) was used for all experiments.

6.2 Methods

Adsorption experiments. Samples for batch adsorption tests were prepared by diluting 1000 ppm gold spectroscopy standard solution in 5% hydrochloric acid. In general, for adsorption experiments, 10 ml of stock solution with 50 ppm of Au(III) concentration were placed in 10 mL plastic tubes, containing 20 mg of N12 powder. The mixture has been shaken for 12h at room temperature on an orbital shaker at 300 rpm. After the adsorption, the solution was filtrated with syringe filters (Phenex RC 0.45 μm) and the filtrate was analyzed by atomic absorption spectroscopy to determine Au(III) concentration. The adsorbent was removed from filter and dried at room temperature for further analysis. The amount of recovered Au(III) (q,%) from the synthetic solution by N12 was calculated by Equation 6.1

$$q = \frac{C_i - C_e}{C_i} \cdot 100\% \quad (6.1)$$

where C_i and C_e are the concentrations of analyte in mg/L before and after Au(III) adsorption respectively.

The amount of Au(III) adsorbed per unit mass of N12 adsorbent was determined by following equation

$$q_t = \frac{(C_i - C_e)}{m} \cdot V \quad (6.2)$$

where q_t is equilibrium adsorption capacity, mg/g; m is a dry weight of adsorbent in g, and V is the volume of a sample in mL.

Different pH. At the beginning, the adsorption behavior of Au(III) onto N12 powder at different pH were investigated. Samples with different pH (0, 0.5, 1, 3, 5, 7, 9) were adjusted by adding HCl and NaOH solutions. A 10 mL of obtained synthetic solutions were placed in 10 ml plastic tubes with 20 mg of N12 powder. The mixture has been shaken for 12h at room temperature on orbital shaker at 300 rpm.

Adsorption isotherms. Adsorption isotherm experiments were performed by mixing 20 mg of N12 powder and 10 mL of synthetic gold solution with initial concentrations varying from 9.5 mg/L to 295.1 mg/L at pH 0. Different equilibrium isotherm models such as Langmuir, Freundlich and Sips were applied to experimental data therefore the physicochemical parameters were obtained. Isotherm model fitting as well as calculations of parameters were done using Microsoft Office Excel 2016. Sum square error (ERRSQ) function was used for minimizing the error function between experimental and calculated data.

Kinetic studies. Adsorption kinetics tests were accomplished for both Au(III) concentrations 30 mg/L and 50 mg/L at pH 0 and room temperature. The amount of N12 powder was 20mg and sample volume was 10 mL. Experimental data were described with Pseudo-first-order, Pseudo-second-order, Elovich, and Intraparticle diffusion models. The obtained adsorption rate constant and ERRSQ function were calculated by Microsoft Office Excel 2016.

Adsorption experiments with AM adsorbent. Adsorption experiments with AM objects were performed by mixing 10 mL of synthetic solution containing 250 mg/L of Au(III) in 5%

hydrochloric acid with the adsorbent placed in 50 mL plastic tube. The shaking was performed on orbital shaker at 300 rpm and room temperature for 12 h. The average mass of samples was 0.8 g.

AM objects manufactured with different scanning speed were tested in order to compare the ability of Au(III) uptake. For this purpose, the effect of different initial concentration was performed for both samples. Adsorption test

Adsorption experiments with a fishing net. The old fishing net was acquired from the household and was washed with deionized water and dried at 55 °C in the oven before the experiments. Dry sample were cut in small pieces with the length rage from 5 to 10 mm and washed with 10 % aqua regia to eliminate any trace metals. After that, the samples were washed again with deionized water and dried in the oven at 55 °C to constant weight. A 10 mL sample of synthetic solution containing 50 ppm of Au(III) was placed in 10 mL tube with 0.1 g of pre-washed fishing net at pH 0. The mixture has been shaking for 12 h at room temperature.

Additive manufacturing of adsorbent. Designing and fabrication of AM objects were done by Materflow Oy, Finland. Additive manufacturing was performed by using EOSINT P 395 system (EOS GmbH, Germany) which utilizes powder bed fusion method and N12 polymer powder. Table 4 reveals parameters used in additive manufacturing. Change in scanning speed allowed the obtaining of more porous sample surface.

Table 4. Operating conditions used for AM of polymer adsorbent.

Layer thickness	Laser power, W		Scanning speed, mm/s		Build chamber temperature	Process chamber temperature
	1st grade	2d grade	1st grade	2d grade		
0.12 mm	32	32	2560	3100	135 °C	176 °C

Solution analysis. After all adsorption experiments, samples were filtrated, and liquid phase was analyzed by atomic absorbance spectroscopy (3300 AAS, Thermo Fischer Scientific, US). The measurements were conducted at wavelength 242.8 nm. Standard solutions with concentrations from 0.25 to 10 mg/L were prepared diluting 1000 ppm gold spectroscopy

standard. Optimization solution contained 12 mg/L of Au(III). The dilution of sample solutions was applied where it was required. Nitric acid (7M) was added (1% v/v) to all samples as well as to standard solutions in order to provide acidic media and prevent metal precipitation.

6.3 Adsorbent characterization

Surface charge. Zeta potential of nylon-12 powder was measured by a SurPASS electrokinetic analyzer (Anton Paar GmbH, Graz, Austria). The measurement was operated by automatic titration with 1 mM KCl solution at room temperature using Ag/AgCl electrodes. The starting point was pH 8 and the measurement was performed until pH 3 was achieved. Zeta potential values were calculated by Helmholz-Smoluchowski using measured streaming potentials.

Fourier Transform Infrared Spectroscopy. Infrared spectra of origin and gold-loaded adsorbents were measured with Perkin Elmer Frontier spectrometer with universal ATR module (Diamond crystal) to identify any differences in polymer structure after adsorption. AM samples were also analyzed with FTIR to confirm no changes in the polymer after laser sintering. Measurements were conducted in a mid-infrared region (4000 to 400 cm^{-1}) with a resolution of 4 cm^{-1}. All spectra were obtained in absorbance mode and certain corrections such as ATR correction, baseline correction and normalization were applied. Gold-loaded samples were prepared by mixing 20 mg of N12 powder with initial Au(III) concentrations of 100 mg/L and pH 0 and pH 9. Fishing net was measured at the same conditions as polymer powder, obtained results were compared to database.

Brunauer-Emmett-Teller Surface Area Analysis. BET method was applied to determine pore volume and surface area of the adsorbents. Three-dimensional polymer objects manufactured with different scanning speed as well as fishing net were characterized by automated gas adsorption analyzer BELSORP Mini II (MicrotracBEL Corp., Japan). Pre-treatment (2h at 105°C) was performed for all samples to prevent degassing during the measurements.

Scanning Electron Microscopy. SEM measurements were performed by Hitachi SU 3500 (Japan) coupled with EDS analysis. The acceleration voltage used was 15kV and high

vacuum conditions were applied during the measurement. Both N12 powder and AM objects were analyzed therefore, morphology of the adsorbent surfaces and element concentration were determined.

X-ray Photoelectron Spectroscopy. XPS analysis was performed by ESCALAB 250Xi system (Thermo Fisher Scientific, US) at Centre for Material Analysis, University of Oulu. Obtained XPS spectra were processed with software package. Both samples native N12 powder and gold-loaded N12 powder were analyzed to determine the presence of C, N, O and gold atoms on the surface. In addition, information about gold chemical state was obtained. Gold-loaded sample was prepared by mixing 20 mg of nylon-12 powder with 10mL of solution with Au concentration of 100 mg/L. Solution has been shaking for 12h at room temperature.

7. RESULTS AND DISCUSSIONS

7.1 Characterization of the adsorbents

Infrared spectroscopy is a widely used technique which determines the structure of the compound based on its ability to absorb (or transmit) infrared radiation. Thereby, the analysis provides the information about the presence of specific element, type of the bond between molecules and the structure of molecule, however, regarding to the latter sometimes additional analysis such as NMR is required. (LCGC's CHROM academy, 2014)

FTIR analysis was performed for both N12 powder and AM sample to prove that after laser sintering during additive manufacturing the polymeric material did not change its functionality. In addition, during PBF process building chamber is loaded with 50% of new powder together with 50% of used one. This is done to reduce material coast as well as material waste (Weijmarshausen, 2014). Thus, it was important to conduct FTIR analysis to ensure polymer structure.

Figure 15 displays FTIR spectra of native N12 powder, AM sample and fishing net. Polyamides such as nylon refers to a secondary amide comprising secondary amide linkage where nitrogen involved in one N-H bond and two C-N bonds (Smith, 1999). The N-H group can be presented as both stretching and bending vibrations. For secondary amides, stretching N-H band located in the range between 3370 and 3170 cm^{-1}. The peak appears in the range of 1680-1630 cm^{-1} indicates C=O stretching of secondary amides. (Han, et al., 2013)

Regarding N-H bend vibration, it can be presented as an in-plane and an out-of-plane band. For secondary amides, the most important is in-plane N-H bend vibration and it reveals a peak between 1570 and 1515 cm^{-1}. (Scott, 1973) The intensity of this peak is usually as strong as the one of C=O stretching. Other groups which attributed to the same wavenumber range are carboxylates and nitro group (Coates, 2006). However, neither of them appears together with carbonyl strong peak. It is useful to note the overtone band at about 3100 cm^{-1} which is appeared by in-plane N-H vibration can also indicate unsaturated C-H stretching band. However, N-H bend band is much widely than most of C-H stretching bands. (Smith, 1999) The out-of-plane N-H bend band appears in the range from 750 to 680 cm^{-1}. This

band is medium-to-weak and less important because it overlaps with the out-of-plane N-H bend band of primary amides. (Scott, 1973) Finally, the secondary amide C-N stretch band occurs from 1310 to 1230 cm^{-1} (Jung, et al., 2018).

Therefore, the distinguish peaks for secondary amides are single N-H stretch band, and C=O stretching band with strong N-H bend in the region from 1570 to 1515 cm^{-1} (Smith, 1999). Table 4 represents peak assignments of polyamides used as adsorbent in current work.

As it was stated before, fishing net was obtained from household, therefore material composition was unknown. Obtained IR spectrum corresponds to the one of nylon-12. However, based on the database of KnowItAll® ID Expert™ software, there is 98% match with nylon-6,6 polymer produced by DuPont. Hence, as it was assumed, fishing net was manufactured by nylon-6,6 polymer and its spectrum revealed that the functionality of the polymer remained. Thereby, there is a possibility to utilize the fishing net as an adsorbent for Au(III) recovery.

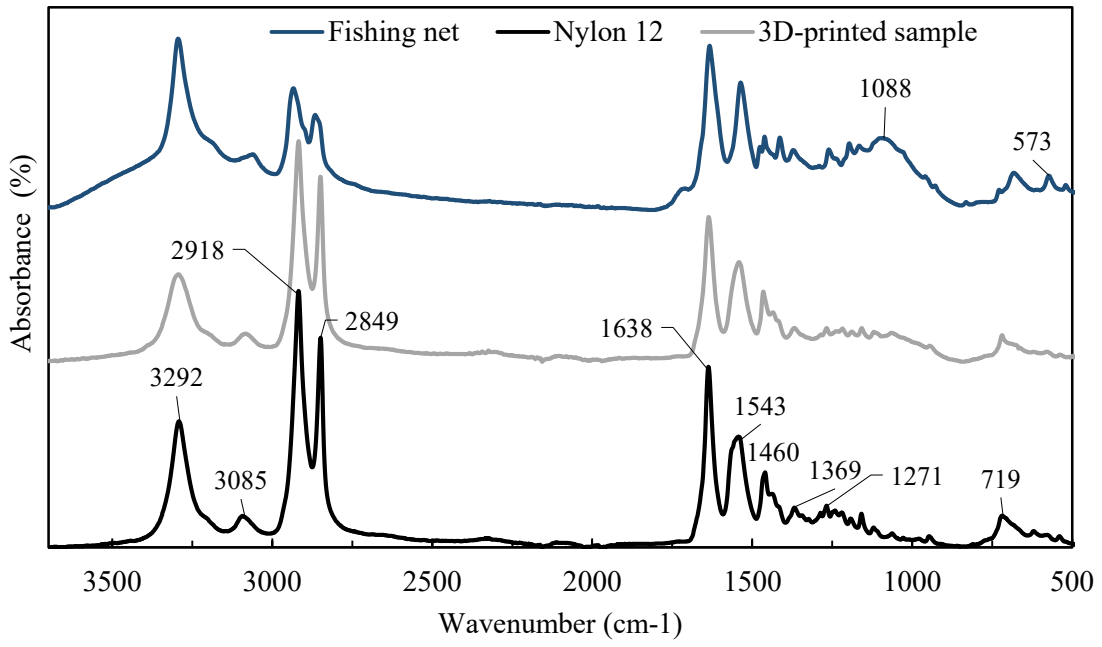

Figure 15. FTIR spectra of N12 powder, AM sample and fishing net.

Table 4. FTIR spectrum of N12 powder. (Smith, 1999; Scott, 1973; Han, et al., 2013)

N12 powder	Peak assignments
3292	N-H stretching

3094	Overtone of N-H bend
2918	CH_2 asymmetric stretching
2849	CH_2 symmetric stretching
1638	C=O stretching
1543	In-plane N-H bend
1460	CH_2 bend
1271	C-N stretching
719	Out-of-plane N-H bend

7.2 Influence of pH on Au(III) adsorption

It is well known that the pH of solution plays a vital role in the adsorption process. Changes in pH values affect the surface charge of the adsorbent as well as speciation of metal ion (Zhao, et al., 2019). Thus, it is important to determine optimal solution pH in order to obtain higher metal removal. Figure 16 (a) reveals the behavior of Au(III) adsorption onto N12 powder at pH range from 0 to 9. As one can notice, adsorption efficiency increases with decreasing of pH and at pH 0 the adsorption capacity reaches the value of 11.84 mg/g. This can be described by the morphology of chloro-gold complex presented in the solution. At lower pH, $AuCl_4^-$ ions have been attracted electrostatically by protonated $-NH_3^+$ groups located on polymer surface (Li, et al., 2013). However, it is also possible, that except electrostatic interaction, ion-exchange can take place between metal ion and the active centers on the adsorbent what can be demonstrated as follows (Mihăilescu, et al., 2019):

$$(R - NH_3^+)Cl^- + AuCl_4^- \leftrightarrow (R - NH_3^+)AuCl_4^- + Cl^- \quad (7.1)$$

At higher pH, the amount of adsorbed Au(III) drops dramatically and at pH 9 the adsorption capacity is 0.085 mg/g. It is useful to note, that with reducing the pH, the color of solution altered from yellow to colorless, showing that the changes in gold speciation occurred (Bond, et al., 2006). This happens due to the hydrolysis of chloro-gold complex in the aqueous chloride solution with subsequent formation of chloride-hydroxide complexes such as $AuCl_3OH^-$, $AuCl_2(OH)^-_2$, $AuCl(OH)^-_3$ and $Au(OH)_3$ (Ogata & Nakano, 2005). Thus, the

competition between Cl^-, $AuCl_4^-$ anions and hydrolyzed chloro-gold complexes occurred. In addition, deprotonation of amino groups at lower pH causes the decrease in electrostatic attraction between Au(III) anions and adsorption sites. (Li, et al., 2013) This can be supported by Figure 16 (b), where the dependence of zeta potential values of N12 powder at different pH is presented. As it can be seen, zero potential charge value pH_{ZPC} of the powder equals 5.1. Thereby, at pH lower than 5.1 the surface of nylon-12 powder contains positive charge whereas at pH above 5.1, the surface charge indicates to be negative.

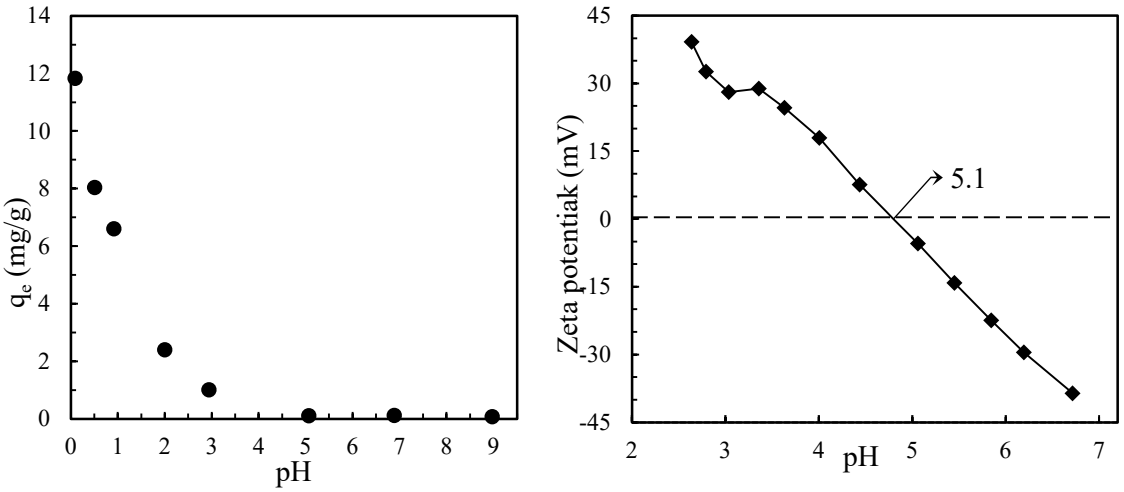

Figure 16 Amount of Au(III) adsorbed onto 20 mg of N12 powder in 10 mL of 50 mg/L Au(III) solution at different pH (a) and Zeta potential values of pristine N12 powder at different pH (b).

7.3 Adsorption of Au(III) on N12 powder

Adsorption kinetics

Figure 7 reveals the effect of contact time for gold adsorption on nylon-12 powder with initial concentrations of solution 30 ppm and 50 ppm. As it can be seen, the adsorption capacity increases with increasing the contact time, however, there is no rapid adsorption and more than 50% removal is achieved after 6h for 30 ppm and 10 h for 50 ppm. The higher initial concentration of the solution, the more contact time is required to obtain equilibrium capacity. Moreover, the amount of Au(III) ions adsorbed on the N12 powder with lower initial gold concentration is lower than the amount of gold adsorbed with higher initial concentration. Figure 17 shows that the adsorption equilibrium was not achieved even after 24 h and the curves are trending. After 24 h 86.3% and 71.3% of Au(III) removal was achieved from the solutions with initial concentrations of 30 ppm and 50 ppm respectively.

The possible explanation is the agglomeration of gold particles on the surface, thereby adsorption sites were not completely occupied.

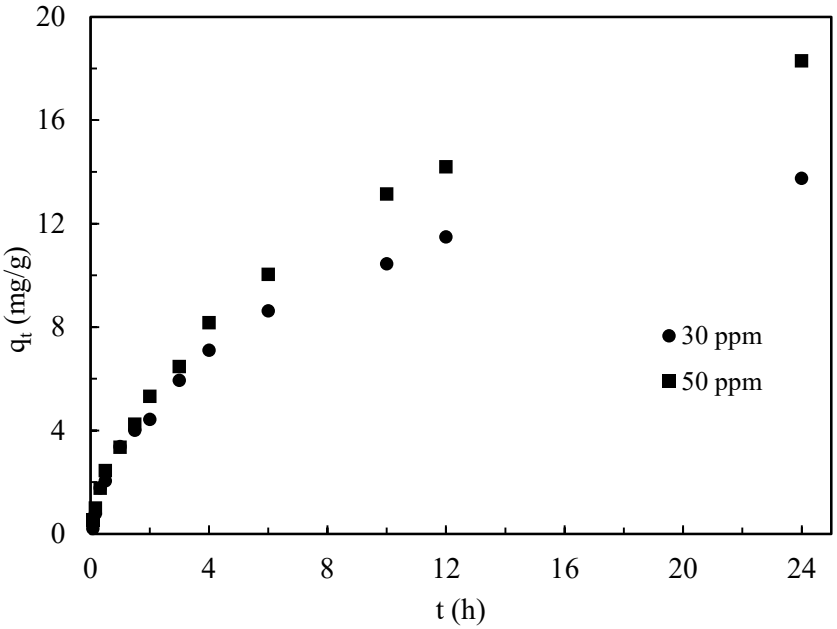

Figure 17. Effect of contact time of Au(III) adsorption onto N12 powder with initial 30 ppm and 50 ppm.

Kinetic performance of Au(III) towards N12 powder was investigated by certain models. Non-linear Pseudo-first order and Pseudo-second order models, as well as Elovich and Intraparticle diffusion models, were applied to determine adsorption kinetic parameters. Calculated kinetic parameters, correlation coefficient r^2 and error function values are presented in the Table 5. According to obtained results, the Pseudo-second-order model correlates better with experimental data than Pseudo-first-order model. Thus, the chemisorption is predominant during the gold adsorption process (Gulnaz, et al., 2005).

Table 5. Adsorption kinetic model parameters

		Initial Au(III) concentration	
		30	50
Pseudo-first-order model	k_1	0.003	0.002
$q_t = q_e(1 - e^{-k_1 t})$	q_t	12.993	17.995
	r^2	0.982	0.986
	$\sum(q_t - q_{model})^2$	4.597	6.065

Pseudo-second-order model $q_t = \frac{q_e^2 k_2 t}{1 + q_e k_2 t}$	k_2	$0.208 \cdot 10^{-3}$	$9.727 \cdot 10^{-5}$
	q_t	16.202	23.287
	r^2	0.993	0.993
	$\sum(q_t - q_{model})^2$	1.834	2.865
Elovich model $q_t = \frac{1}{B_e} ln(1 + A_e B_e t)$	B_e	0.236	0.150
	A_e	0.076	0.067
	r^2	0.997	0.997
	$\sum(q_t - q_{model})^2$	0.884	1.372
Intraparticle diffusion model $q_t = k_{dif} t^{1/2} + C$	k_{dif}	0.402	0.503
	C	0.088	$7.231 \cdot 10^{-12}$
	r^2	0.977	0.990
	$\sum(q_t - q_{model})^2$	5.872	4.180

However, Elovich model fitting shows higher r^2 value equals to 0.997 for both initial concentrations and lower error function value which is 0.884 for 30 ppm solution and 1.372 for 50 ppm solution. Thus, the Elovich model was better than PS1, PS2 and Intraparticle diffusion models to fit the adsorption kinetics of gold ions onto polymer powder. Figure 18, 19 depicts the adsorption kinetics for Au(III) on N12 powder with initial solution concentrations of 30 ppm and 50 ppm.

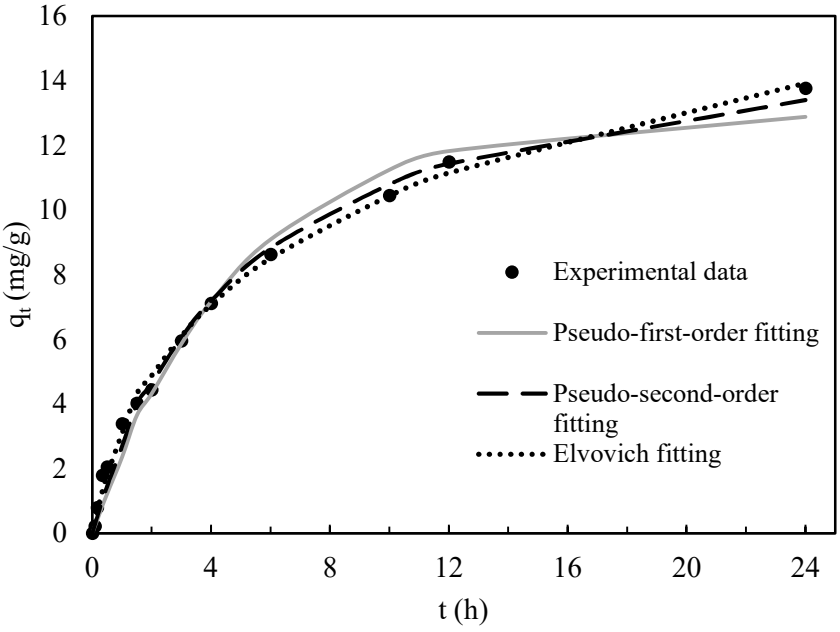

Figure 18. Sorption kinetics of Au(III) with initial concentration 30 ppm on N12 powder and fitting by Pseudo-first-order, Pseudo-second-order and Elovich models.

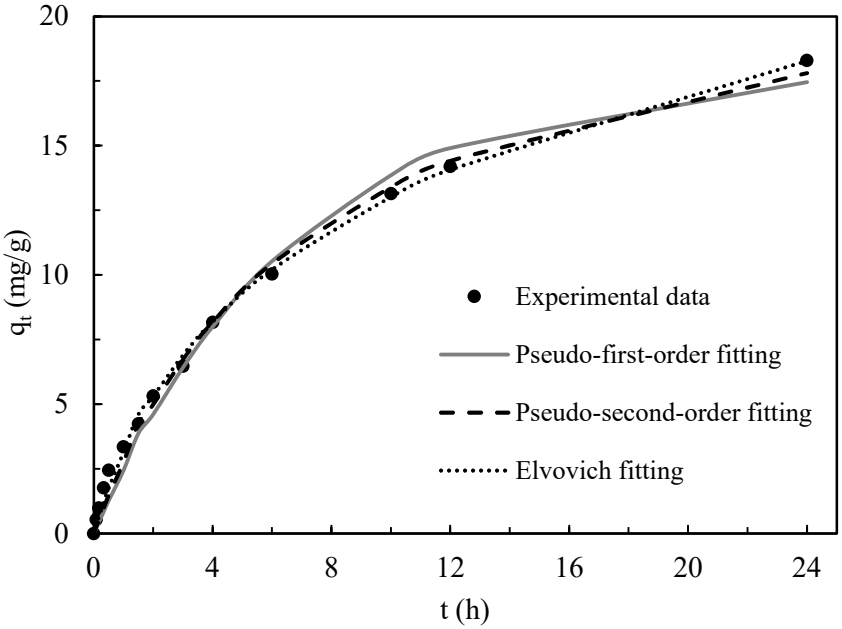

Figure 19. Sorption kinetics of Au(III) with initial concentration 50 ppm on N12 powder and fitting by Pseudo-first-order, Pseudo-second-order and Elovich models.

Figure 20 shows the Intraparticle diffusion model plotted by q_t versus $t^{0.5}$ and its fitting to to the obtained data for solutions with concentration of Au 30 ppm (a) and 50 ppm (b). As it can be seen, the plotted line is not straight and do not go through the origin in both cases. In addition, the correlation coefficient r^2 is equal to 0.977 for 30 ppm solution and 0.990 for 50 ppm solution. The SSE values are 5.872 and 4.180 for 30 ppm and 50 ppm solutions respectively which are higher than in the case of other models. This indicates that Intraparticle diffusion is not a controlling step in adsorption of Au(III) on N12 powder.

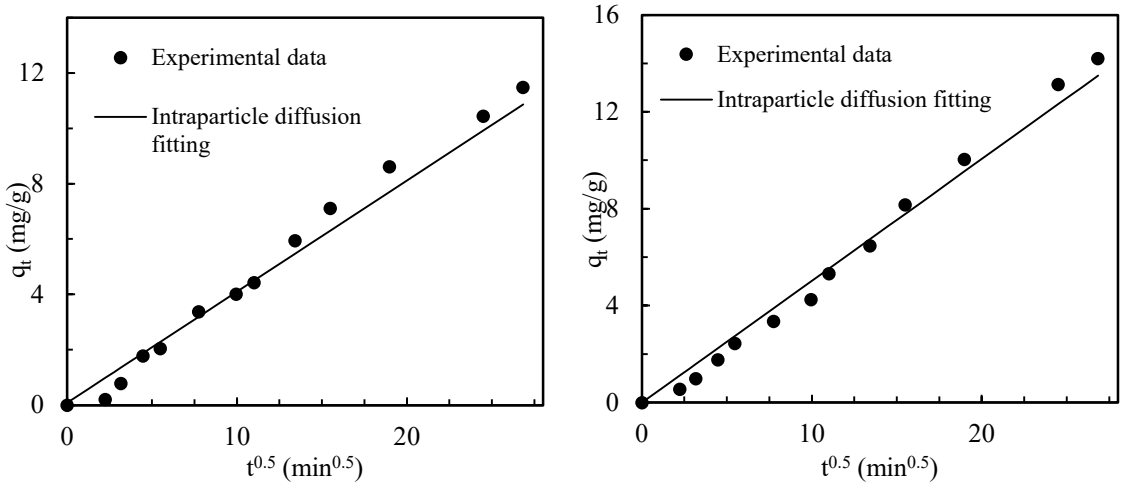

Figure 20. Sorption kinetics of Au(III) with initial concentration of 30 ppm (a) and 50 ppm (b) on N12 powder and fitting by Intraparticle diffusion model.

Adsorption isotherms

Nonlinearized Langmuir, Freundlich isotherms models and Sips model were used to analyze experimental data. The model fitting curves and obtained isotherm parameters including their correlation coefficients and residual standard deviations are presented in Figure 21 and Table 6. Adsorption isotherms represent L-type isotherm with no strict plateau indicating a progressive saturation (Repo, 2011).

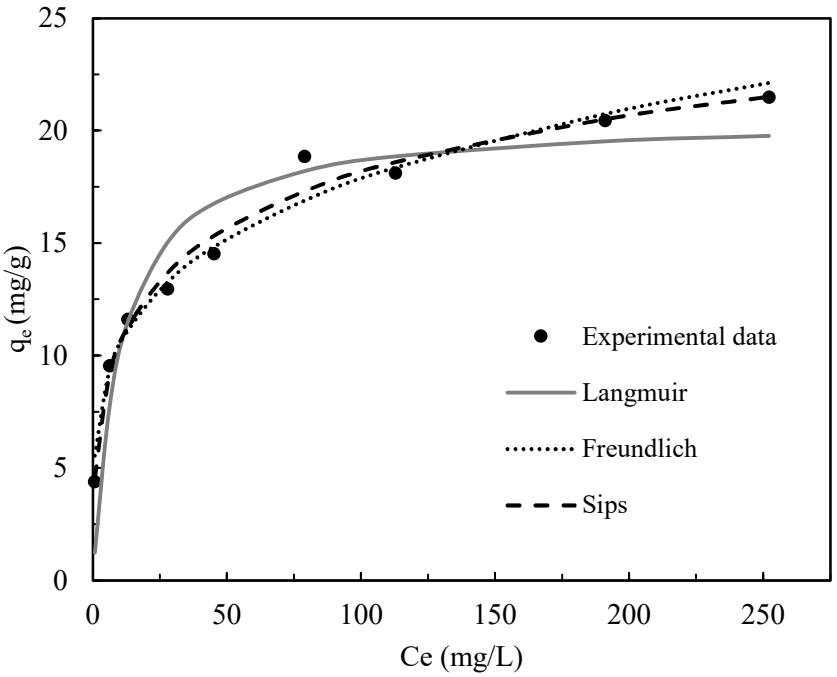

Figure 21. Nonlinearized isotherms for Au(III) adsorption by N12 powder at room temperature.

The results display that experimental data could not be fitted well to Langmuir model according to r^2 value which is equal to 0.892. The monolayer capacity of N12 powder at room temperature is 19.77 mg/g. Langmuir parameter K_L refers to affinity between adsorbate and binding sites and for N12 powder is 0.0971. Adsorption is considered as favorable if $0 < K_L < 1$ (Fierro, et al., 2008).

In contrast, Freundlich model correlation parameter r^2 is 0.993 indicating better fitting. In addition, the adsorption capacity value is 22.13 mg/g what is closer to experimental data. Therefore, it can be assumed that Au(III) binding follows heterogeneous adsorption by a multilayer adsorption mechanism. Freundlich constants K_F and n corresponds to the adsorption capacity and energetic heterogeneity of the adsorbent respectively (Blázquez, et

al., 2011). Freundlich parameter n is equal 4.305 what indicates satisfactory adsorption process, since the value within the range from 1 to 10 (Fierro, et al., 2008).

Table 6. Adsorption isotherms parameters

Langmuir model	q_m	20.581
$q_e = \frac{q_m K_L C_e}{1 + K_L C_e}$	K_L	0.097
	r^2	0.892
	$\sum(q_t - q_{model})^2$	27.290
Freundlich model	K_F	6.125
$q_e = K_F C_e^{1/n}$	n	4.305
	r^2	0.993
	$\sum(q_t - q_{model})^2$	6.194
Sips model	K_S	0.007
$q_e = \frac{q_m (K_S C_e)^{n_S}}{1 + (K_S C_e)^{n_S}}$	q_m	38.930
	n_S	0.375
	r^2	0.996
	$\sum(q_t - q_{model})^2$	4.068

The Sips equation describes experimental data better than Langmuir and Freundlich ones. It exhibits higher value of r^2 (0.996) and lower value of ERRSQ (4.068). Sips isotherm is a combination of Langmuir and Freundlich isotherms. Thus, n_S constant can determine the heterogeneity of adsorption sites. If n_S value is closer to unity, the isotherm tends to be considered as Langmuir isotherm with homogeneous adsorbent. However, deviation of n value from unity represents heterogeneous adsorption cites with multilayer adsorption. (Hokkanen, et al., 2017) From Table 6, Sips constant n_S is equal 0.375, hence recovery of Au(III) on N12 powder indicates possible multilayer adsorption on heterogeneous surface of adsorbent.

7.4 Adsorption of Au(III) on AM adsorbent

Adsorption kinetics

Effect of contact time on adsorption of Au(III) onto AM adsorbent at different temperatures was observed. The initial concentration of gold in the solution was set as 233mg/g. Figure

22 shows that at temperature 333 K metal uptake is more rapid at the beginning than at lower temperatures. Therefore, after 1h the adsorption capacity reached the value of 3.12 mg/g whereas for 296 K and 313 K only 0.35 mg/g and 1.55 mg/g respectively. However, after fast saturation of adsorption cites the adsorption capacity dropped slightly until the equilibrium was reached. At both temperatures 313K and 333K, the adsorption equilibrium was achieved after 6 h and equal to 2.48 mg/g and 2.39 mg/g respectively. However, at temperature 296 K the adsorption capacity of AM nylon was reached only after 24h. Clearly, temperature has an impact on adsorption kinetic, however, it is useful to note, that that at temperature 313 K, the capacity is slightly higher than at 333K. Therefore, increasing temperature up to 333K is inefficient.

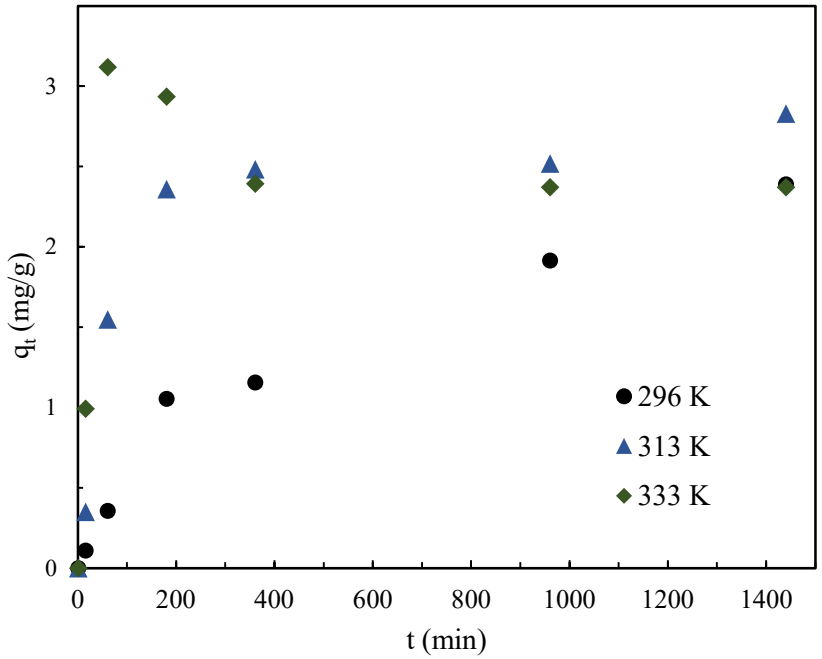

Figure 22. Effect of contact time on adsorption of Au(III) on AM adsorbent at different temperatures.

The adsorption kinetics of gold on the AM polymeric objects is reveled in Figure 23, 24. Obtained experimental data was fitted by several model equations. Table 7 exhibits kinetic parameters of Pseudo-first order, Pseudo-second order, Elovich and Intraparticle models at different temperatures. Raising the temperature cause the increase in rate parameters however, residual standard deviation also increasing. Experimental data measured at 296 K can be well described by Elovich kinetic model. The regression coefficient is 0.987 and the SSE value is 0.066. In addition, calculated amount of adsorbed gold ions at equilibrium was in the good agreement with the experimental values. At higher temperatures, Pseudo-first

order model equation shows better fitting for obtained data with r^2 equals to 0.988 for 313K and 0.892 for 333K. Based on this, it may be suggested that physical adsorption is the rate limiting step in the recovery of Au(III) on AM N12 adsorbent.

Table 7. Adsorption kinetic model parameters for AM samples at different temperatures.

		Temperature, K		
		296	313	333
Pseudo-first-order model $q_t = q_e(1 - e^{-k_1 t})$	k_1	0.002	0.014	0.046
	q_t	2.331	2.615	2.630
	r^2	0.971	0.988	0.892
	$\sum(q_t - q_{model})^2$	0.144	0.094	0.814
Pseudo-second-order model $q_t = \frac{q_e^2 k_2 t}{1 + q_e k_2 t}$	k_2	$0.730 \cdot 10^{-3}$	0.006	0.032
	q_t	2.993	2.869	2.698
	r^2	0.981	0.978	0.814
	$\sum(q_t - q_{model})^2$	0.096	0.140	1.405
Elovich model $q_t = \frac{1}{B_e} ln(1 + A_e B_e t)$	B_e	1.193	1.989	5.651
	A_e	0.009	0.129	536.890
	r^2	0.987	0.933	0.694
	$\sum(q_t - q_{model})^2$	0.066	0.519	2.315
Intraparticle diffusion model $q_t = k_{dif} t^{1/2} + C$	k_{dif}	0.314	0.494	0.368
	C	$0.397 \cdot 10^{-8}$	$0.558 \cdot 10^{-7}$	0.738
	r^2	0.833	0.874	0.484
	$\sum(q_t - q_{model})^2$	0.837	0.971	3.908

Intraparticle diffusion model fitting is showed graphically in Figure 22 (b). As it can be seen, the plot represents multilinearity meaning that two or more stages are involved in the adsorption process (Wu, et al., 1999). At temperature 296 K the plot does not pass the origin and three steps of adsorption process can be identified, however, the r^2 value is low suggesting that internal diffusion is not a controlling step. Regarding adsorption at higher temperature, at 313 K and 333 K two different stages can be observed, meaning that internal diffusion occurred together with surface adsorption (Feng, et al., 2018). Since fitting curves

were off the origin, intraparticle diffusion was not a limited step for adsorption at higher temperatures either.

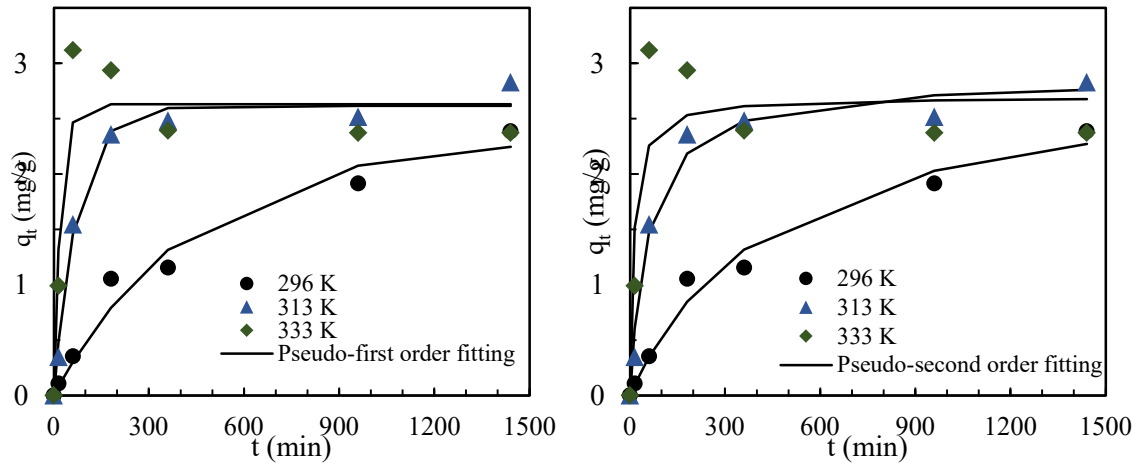

Figure 23. Sorption kinetics of Au(III) on AM adsorbent at different temperature and fitting by Pseudo-first order (a), Pseudo-second order (b).

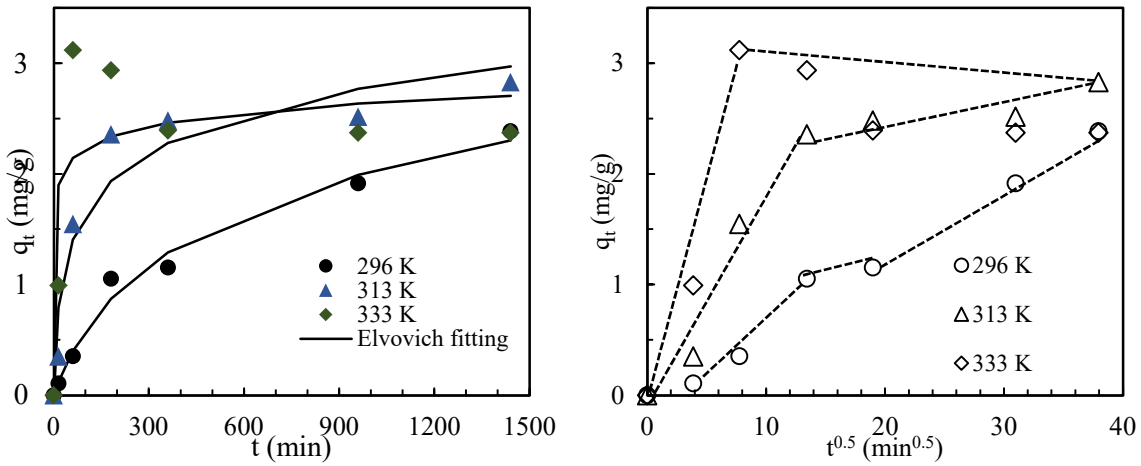

Figure 24. Sorption kinetics of Au(III) on AM adsorbent at different temperature and fitting by Elovich model (a), Intraparticle diffusion model (b).

It is useful to note, that during the adsorption nylon-12 adsorbent tends to change its color (Figure 25). After adsorption at room temperature, AM adsorbent takes the yellow color of gold solution and only the intensity of the color is changing depending on the adsorption time. This can be explained by the amount of gold transferred from the liquid phase towards polymer surface. However, at higher temperatures the color was changed from yellow to purple. The possible explanation is the formation of gold nanoparticles Au_{np} on the surface of adsorbent, which can differ by the size and shape thereby the optical properties may vary. Synthetic gold solution reflects the yellow color whereas nanoscale gold tends to revel the

red color (Faraday, 1857). Addition of salt such as sodium chloride during the gold particles aggregation, changes its red color to purple (Pluchery, et al., 2013).

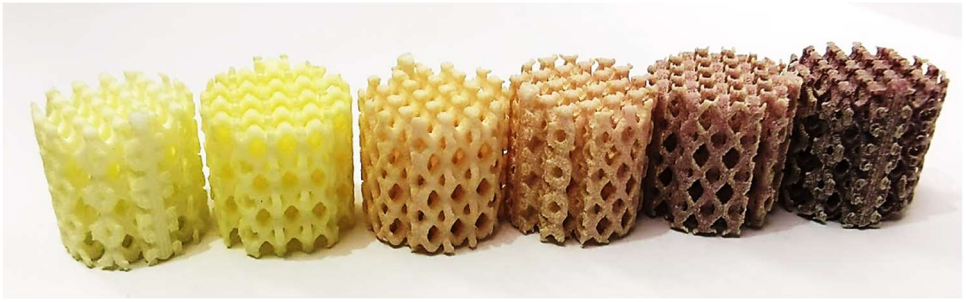

Figure 25. AM nylon-12 adsorbent after adsorption at 333K at different contact time.

Gold-loaded AM adsorbent with different colors were tested with SEM. Figures 26 (a), (b), (c), (d) shows gold aggregations occurred on the surface of nylon-12. Although it is clear that gold has been reduced to the gold nanoparticles, it is tricky to see the tendency in the size of nanoparticles changing with the color.

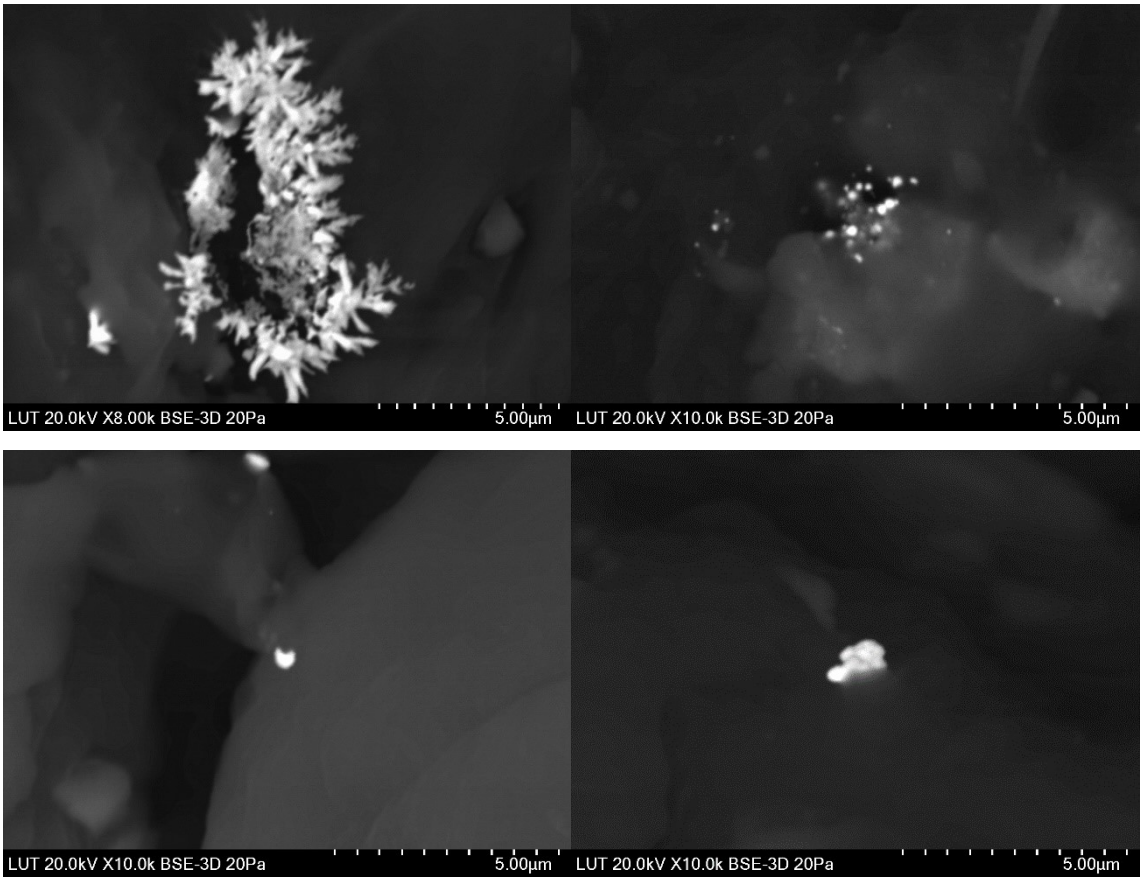

Figure 26. SEM pictures of N12 adsorbent after adsorption at different contact time (a) 15 min, (b) 1 h, (c) 6 h, (d) 24 h at temperature 333K.

Adsorption isotherm

Figure 27 presents the adsorption isotherms of gold ions on additive manufactured nylon-12 adsorbent at room temperature. Non-linear Langmuir and Freundlich isotherm models as well as Sips model were applied to characterize the adsorption of Au(III) on the AM adsorbent and calculated parameters with regression coefficient and residual standard deviations are shown in Table 8. Figure 28 shows color changes of AM samples after adsorption at room temperature with different initial gold concentrations in the solution.

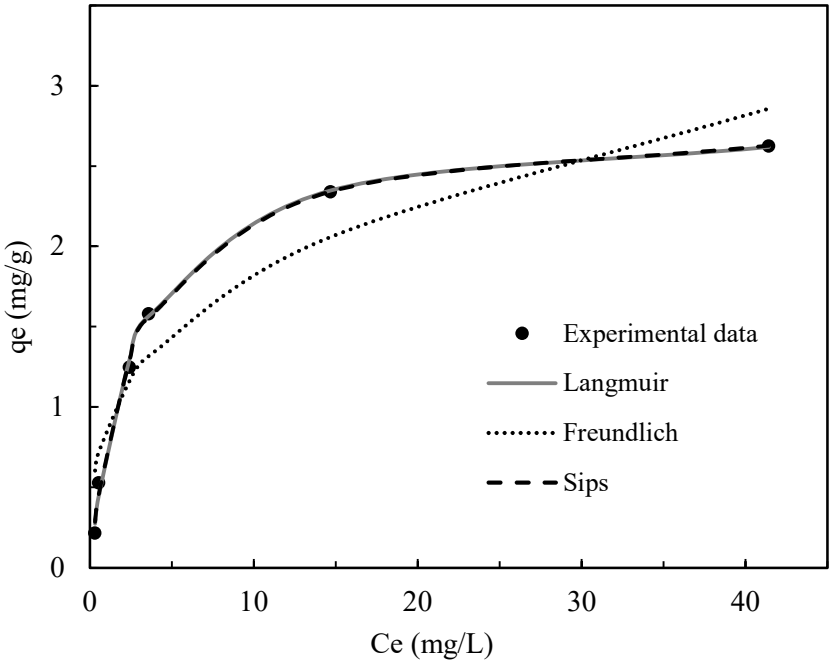

Figure 28. Nonlinearized isotherms for Au(III) adsorption by AM N12 adsorbent at room temperature.

According to the results, both Langmuir isotherm and Sips isotherm exhibit the highest regression value which is equal to 0.997 unlike the Freundlich isotherm (0.914). Langmuir parameter K_L indicating the affinity between the adsorbate and adsorbent is equal to 0.355 which is higher than K_L of gold adsorption on N12 powder. The monolayer capacity of AM N12 objects is 2.63 mg/g. Since Sips constant n_S is closer to unity and equal to 0.969, it is tends to Langmuir isotherm therefore the adsorption of Au(III) on AM adsorbent is considered as monolayer adsorption with rather homogeneous adsorbent.

Table 8. Adsorption isotherms parameters

Langmuir model	q_m	2.798

$q_e = \frac{q_m K_L C_e}{1 + K_L C_e}$	K_L	0.355
	r^2	0.997
	$\sum(q_t - q_{model})^2$	0.013
Freundlich model	K_F	0.880
$q_e = K_F C_e^{1/n}$	n	3.162
	r^2	0.914
	$\sum(q_t - q_{model})^2$	0.397
Sips model	K_S	0.345
$q_e = \frac{q_m (K_S C_e)^{n_S}}{1 + (K_S C_e)^{n_S}}$	q_m	2.827
	n_S	0.969
	r^2	0.997
	$\sum(q_t - q_{model})^2$	0.013

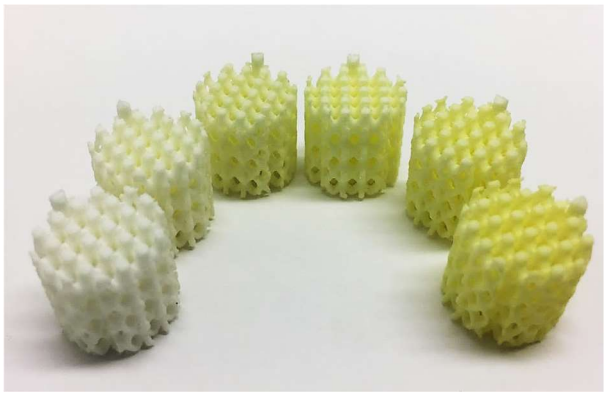

Figure 28. AM samples after adsorption at room temperature with initial concentrations in the range from 20 mg/L to 250 mg/L.

7.5 Comparison of different AM samples

Mechanical and structural properties of additive manufactured materials depend on the manufacturing parameters such as temperature, laser power, scanning speed, layer thickness and build orientation (Flodberg, et al., 2018). Adjusting scanning speed during PBF process helps to achieve desired surface of final product. From mechanical point of view, it is more reasonable to use lower scanning speed, therefore providing fully fusion of powder particles and as a result more rigid structure. However, in term of adsorption, porous structure is more favorable due to increasing the surface area and providing availability of adsorption cites.

Hence, higher scanning speed will help to achieve more friable structure of the adsorbent even though it will be more fragile.

Table 9 displays the characteristics of nylon-12 adsorbents produced with higher and lower scanning speed. BET and BJH methods were applied to observe the differences in surface area and pore size distribution. As one can see, the pore dimeter decreased with increasing scanning speed. Consequently, surface area of the sample grown as well. SEM pictures show that surface morphology was different, and sample printed with lower scanning speed comprised smoother surface (Figure 29).

Table 9. Characteristics of AM samples manufactured with different scanning speed.

Adsorbent	BET surface area (m^2/g)	Total pore volume (cm^3/g)	Mean pore diameter (nm)
Old	0.086	0.006	294.90
New	0.428	0.015	141.80

Nylon-12 adsorbents manufactured with two different scanning speed were used for adsorption tests to observe the difference in adsorption capacity of Au(III) on the polymer. Figure 30 reveals the effect of initial concentrations of gold solution on adsorption efficiency of AM nylon-12 adsorbent produces with lower (a) and higher (b) scanning speed. Clearly, more porous structure allows to achieve higher adsorption capacity of the material. Capacity of the material manufactured with higher scanning speed was double higher and equals 5.42 mg/g whereas adsorption capacity of adsorbent printed with lower scanning speed was 2.03 mg/g.

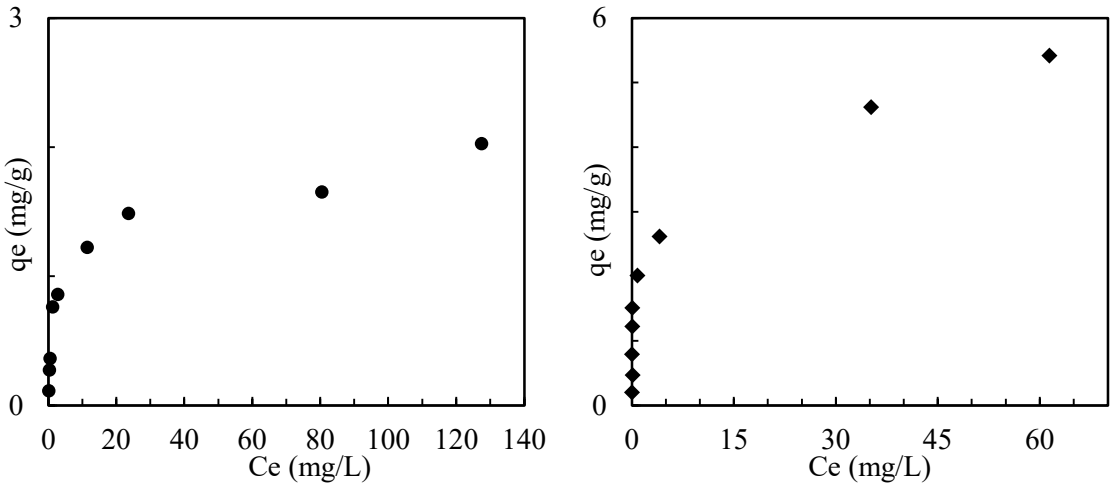

Figure 30. Adsorption capacity of Au(III) on AM adsorbent manufactured with (a) higher laser speed (b) lower laser speed.

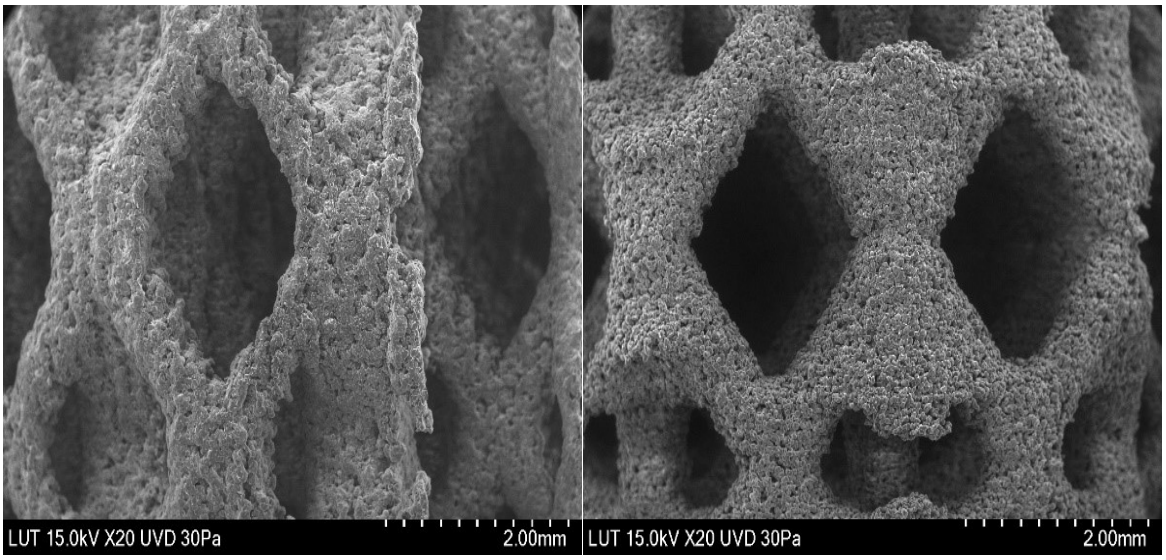

Figure 29. SEM pictures of AM samples with (a) lower and (b) higher scanning speed.

7.6 Adsorption of Au(III) on Fishing net

Acid-washed fishing net was cut randomly in small pieces with the length range from 5 to 10 mm (Figure 31). Table 10 shows the adsorptive removal of Au(III) from aqueous chloride solution at room temperature. The maximum adsorption capacity achieved was equal to 19.3 mg/g and the BET surface area of fishing net was 0.260 m^2/g.

Figure 31. Fishing net used as adsorbent for gold adsorption.

Removal efficiency of Au(III) onto fishing net manufactured from nylon-6.6 decreased with increasing of initial gold concentration in the solution (Table 10). The possible explanation is that at lower gold concentration the availability of adsorption cites is higher. Thus, the percentage of gold removal is decreasing whereas the adsorption capacity is raising.

Table 10. Removal of Au(III) from the synthetic solution with fishing net.

C_{in}, mg/L	Removal, %	q_e mg/g
29.38	99.29	2.91
48.17	98.89	4.75
70.38	99.23	6.96
99.35	99.11	9.83
194.90	99.05	19.31

Nevertheless, the adsorption of Au(III) onto old fishing net was successful even though it was manufactured using nylon-6,6 instead of nylon-12. That means that in the future, it is possible to achieve plastic reuse by collecting fishing nets from household or water media like lakes or seas and use it as an adsorbent for rare metal recovery. The possible route is to place washed and cut fishing net into the extruder and produce filaments for material extrusion machine. Second step will be choosing the right design, and possible modification of the polyamide before or after printing to achieve higher metal recovery by adding active functional group to polymer structure.

7.7 Adsorption mechanism

To understand the possible adsorption mechanism of Au(III) on nylon-12 polymer the material was analyzed by FTIR, SEM and XPS before and after adsorption. FTIR analysis of nylon-12 powder before and after adsorption at both pH 0 and pH 9 are presented on Figure 32. In FTIR spectrum of N12 powder the peak at 3292 cm^1 corresponds to stretching NH group. The region above 3110 cm is also useful for determining of existence of hydrogen bonds. In general, a band in the range 3400-3460 is thought to arise from a free amide proton, and a band in the range 3120-3320 from a hydrogen bonded amide proton. The integrated intensity of these two bands can yield the relative number of free and hydrogen bonded amide protons. When there is a decrease in intensity of the peak which is responsible for hydrogen bonding, intermolecular hydrogen bonding occurs. Moreover, the peak at 1552 cm^{-1} for the secondary amine groups on N12 was shifted to 1539 cm^{-1} after the adsorption of Au(III) at ph = 0 indicating the interaction between gold ions with nitrogen atom in NH group. However, the peak assigned to C=O groups at wavenumber 1638 cm^{-1} was not shifted. Thus it may be suggested that carbonyl groups in amide linkage were not involved in the gold adoption on nylon-12 powder.

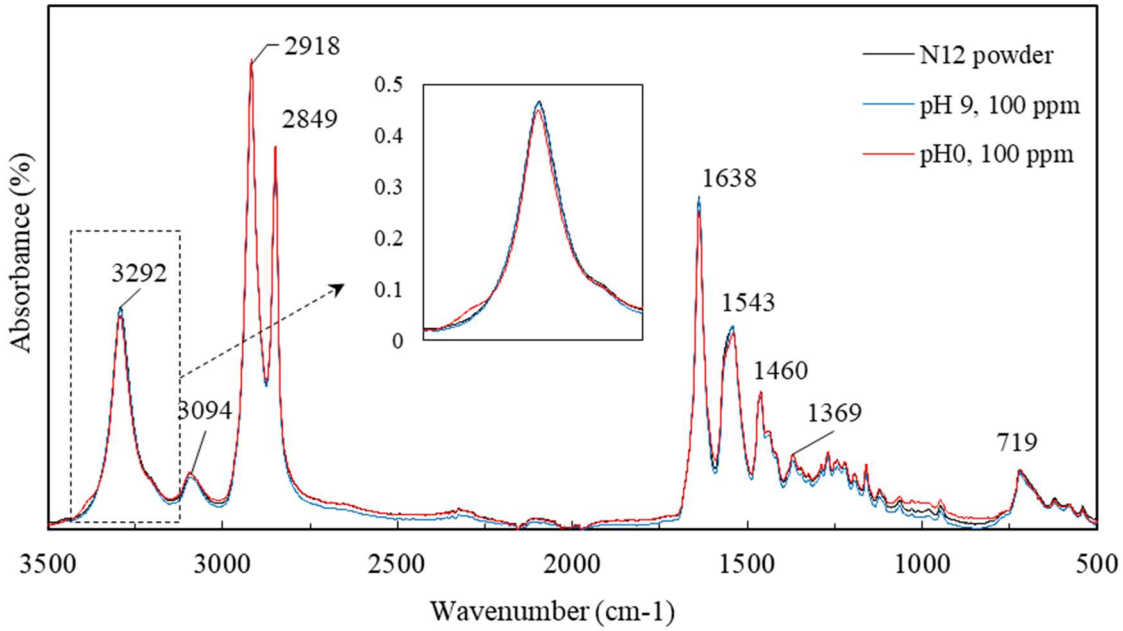

Figure 32. FTIR spectra of N12 powder before and after adsorption at pH 0 and pH 9.

SEM pictures of both N12 powder and AM samples reveals that gold was reduced on the surface of the polymer (Figure 33). At higher temperature during adsorption, gold

agglomerates were presented. Since FTIR spectrum didn't reveal changes in polymer functionality which could possibly be involved in redox reaction with gold chloro-complex, it may be assumed, that other factors influenced on gold reduction such as light, temperature and contact time. It should be considered as well that during PBF manufacturing the N12 powder is a mixture of used powder and a new powder, hence it is difficult to track the exact composition. EDS analysis revealed the presence of the elements such as Co, Cr, Mg, Al, Si, Ti on some of the samples with different concentrations. Thus, there is a chance that these elements can act as a catalyst during the redox reaction. In addition, based on EDS results the polymer samples after adsorption contained gold in the area although there were no visible particles on some SEM pictures. That may also indicate that partially gold was involved in complex formation with some available nitrogen presented in nylon polymer.

XPS analysis is being used for identification of element's chemical state presented on the material surface. Thus, the interaction between metal ions with the active groups presented on the adsorbent's surface may be identified. Once the chemical bond forms between metal ions and an ion on the surface of the solid, it affects the electron clouds around atoms. Thus, donor ligands tend to decrease the binding energy whereas electron acceptor ligands usually rise their binding energy. (Deng, et al., 2003).

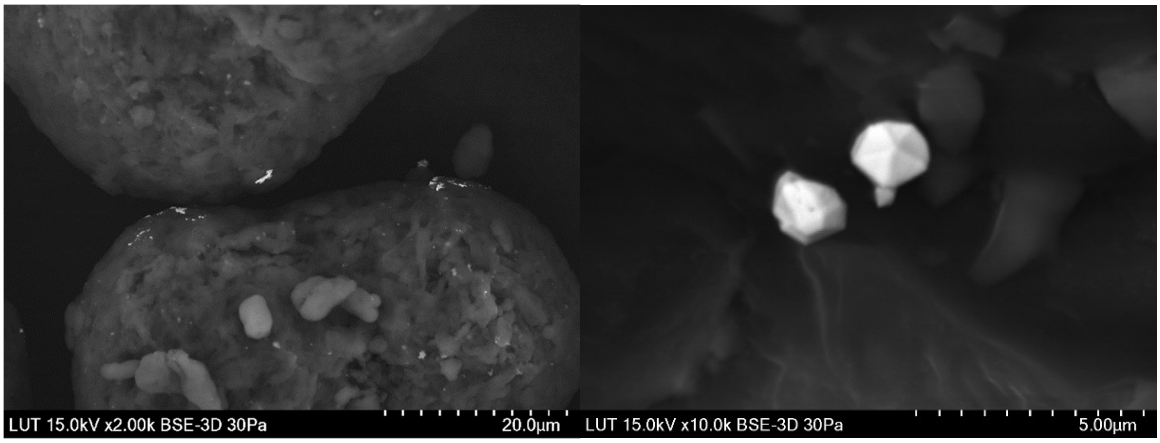

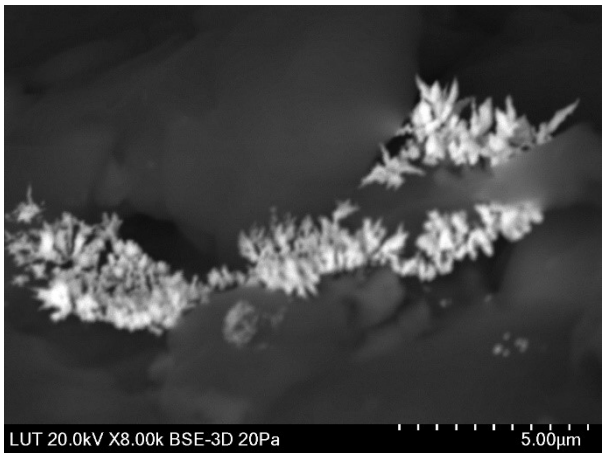

Figure 33. SEM pictures of metallic gold particles on (a) N12 powder and (b), (c) 3-D printed adsorbent.

Survey scan of native nylon-12 powder showed three peaks which defined as for C1s, N1s and O1s respectively (Figure 34). However, new peaks appeared on the spectrum of nylon-12 after adsorption of gold which can be assigned to Au 4d3, Au 4d5, Au4f, and to Cl2s and Cl2p. The O1s, N1s and C1s core spectra of native N12 and N12 after Au adsorption are compared in Figure 35. As it can be seen in Figure 35 (a), the C1s core level XPS spectra can be fitted by three peaks. Peak at 284.91 eV corresponds to interactions of aliphatic carbons such as C–C and C–H (Novak, et al., 2006). Peak at binding energy equals to 285.78 eV attributes to carbon atoms bonded to the –NH– groups and the peak at 287.8 eV assigned to carbon atoms involved in carbonyl groups C=O (Zorn, et al., 2014). After the adsorption of Au on N12powder no significant changes in the peaks can be observed. The O1s spectrum of N12 powder can be fitted in two peaks: 531.19 eV assigned to oxygen atoms presents in carbonyl groups C=O on the polymer surface; and 532.69 eV corresponds to interaction between oxygen and carbon atoms C–O (Kerber, et al., 1996). After the adsorption of gold ions no changes in binding energy was noticed.

Deconvolution of N1s peak at 399 eV reveals two peaks (Figure 35a). The first one at binding energy of 399.49 eV can be attributed to the nitrogen in C–N interaction (Chan, et al., 1990). Another one appears at 400.05 eV can be assigned to N–H groups and three amine groups (Jermakowicz-Bartkowiak, et al., 2003). After adsorption of Au(III) on N12 powder no new peaks were observed (Figure 35b), however the intensity of peak at BE of peak at 400.05 was increased. Sample composition on the polymer surface presented in Table 11.

As it can be seen from the table 16, content of N–H is almost double higher after gold adsorption.

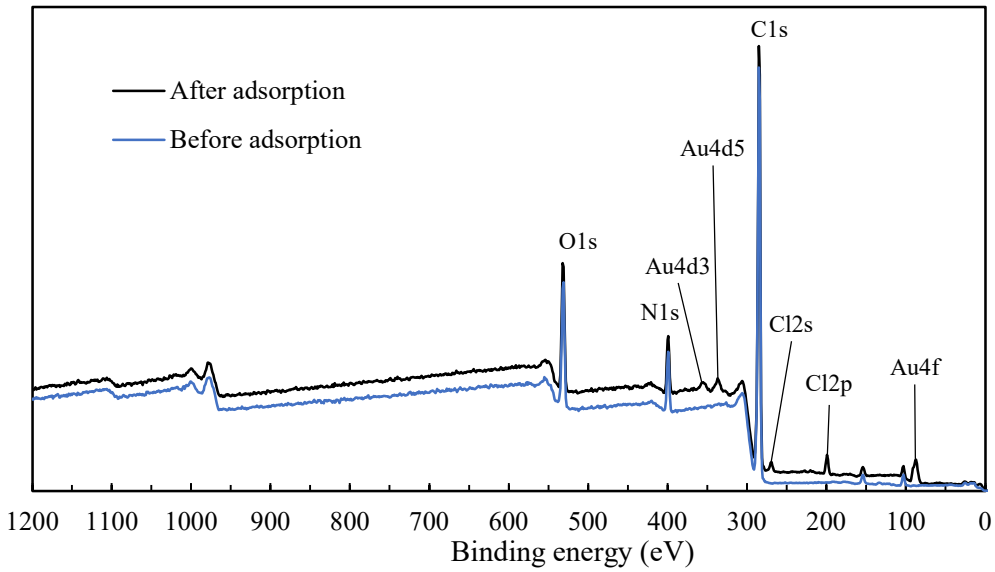

Figure 34. XPS spectra of N12 powder before and after adsorption of Au(III).

Table 11. XPS surface composition on nylon-12powder.

		N12 powder	N12 powder loaded with Au(III)
		Atomic (%)	Atomic (%)
C 1s	C-CH_2-C	57.41	54.7
	C-CH_2-NH	7.26	5.39
	C=O	18.32	22.71
N 1s	C–N	3.89	2.12
	N–H	2.7	4.37
O 1s	C=O	4.96	4.36
	C–O	5.45	5.94
Au 4f7	Au+	-	0.41

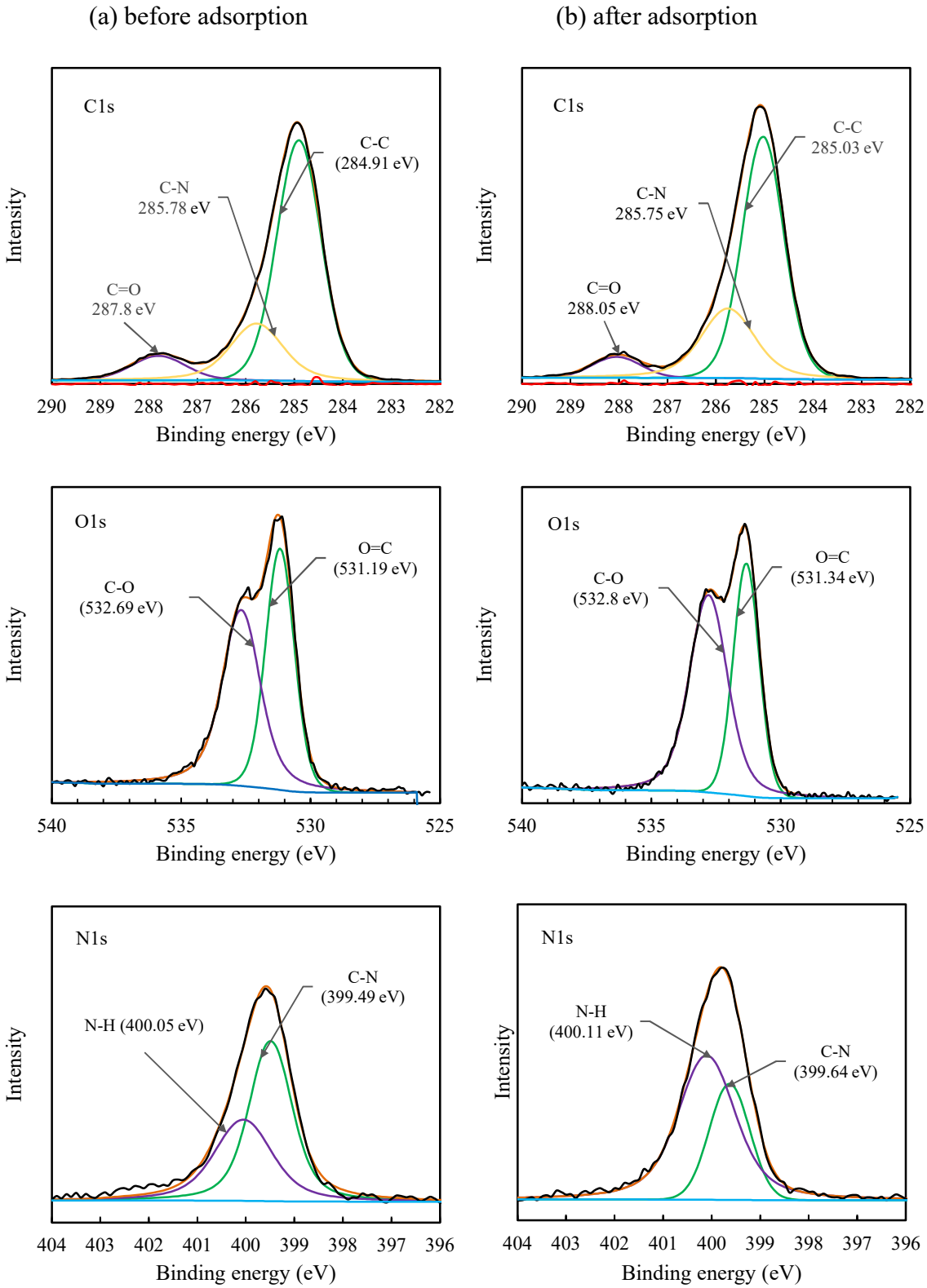

Figure 35. XPS spectra of C1s, O1s and N1s for nylon-12 powder before (a) and after (b) adsorption of Au(III).

Figure 36 demonstrates high-resolution XPS Au4f spectrum. The fitted peak located at 84.1 eV assigned to Au(0) whereas the peak at 87.3 eV assigned to Au(III) and peak at 84.95

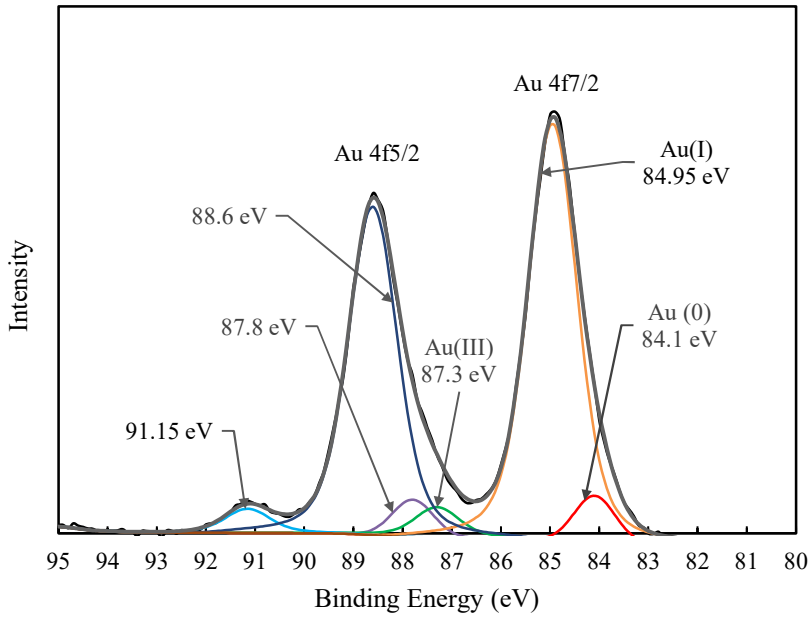

Figure 36. XPS spectrum of Au4f for nylon-12 powder after Au(III) adsorption.

corresponds to Au(I). According to the calculated sample composition, the amount of both Au(0) and Au(III) are very low, indicating that gold reduction is not an adsorption mechanism. Meanwhile, the majority of the gold presented on the nylon-12 surface is in the state of Au(I). This can be explained by the complex transformation of Au(III) to Au(I) due to certain factors such as ligand substitution or redox reactions. Regarding redox transformations, gold specimens Au(III), Au(I) and Au(0) tend to convert into each other based on the effect of reducing agents, coexisting ligands, electrolytes, and pH, resulting in Au complexes with varying standard redox potentials in water. Thus, only a minor part of gold was reduced to Au(0), whereas most of the Au(III) was reduced to Au(I). Therefore, the possible adsorption mechanism of Au(III) on nylon-12 powder is suggested in Figure 37. When N12 adsorbent was added to the synthetic gold solution, Au(III) was firstly adsorbed on the surface of nylon-12 by electrostatic attraction, and then due to external factors, it was reduced to both Au(0) and Au(I).

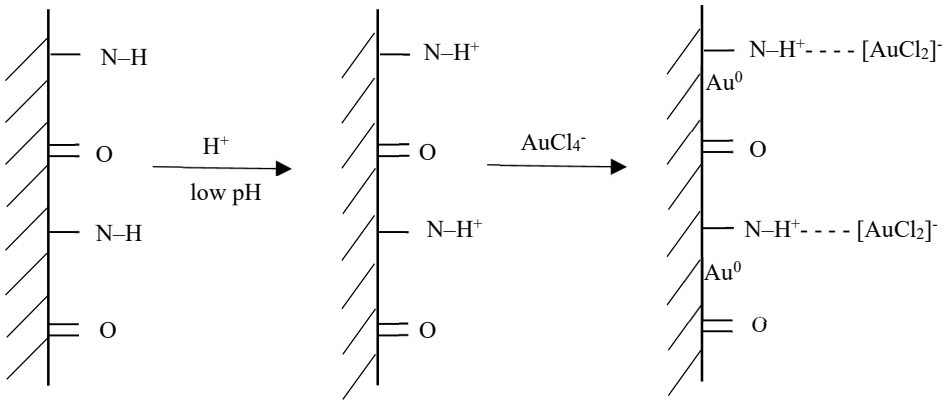

Figure 37. Suggested adsorption mechanism of Au(III) on nylon-12.

8. CONCLUSIONS

This work showed the efficiency of gold adsorption on the polymer adsorbent from synthetic solution. Nylon-12 powder as well as AM nylon-12 adsorbents were tested for Au(III) recovery. It was found that pH of the solution as well as adsorption temperature affect the adsorption significantly. The maximum Au(III) adsorption capacity at room temperature is equal to 21.49 mg/g. Solution pH was set to zero and the adsorption time was 12h. Obtained adsorption isotherm data were well fitted by Sips model whereas the adsorption kinetic data were described by the Elovich model.

Nylon-12 adsorbent manufactured by PBF technology was used for gold recovery. The maximum adsorption capacity value of 2.83 mg/g was achieved at 313K after 16h. Raising the temperature helped to achieve the equilibrium in a shorter time and enhanced adsorption capacity of the adsorbent. Experimental data showed a good fitting with Langmuir and Pseudo-first order models. Increasing the scanning speed parameter contributed in production of more porous objects what lead to enhancing the surface area of the adsorbent. Thus, the BET surface area of AM absorbents with lower scanning speed was equal to 0.086 m^2/g whereas the objects produced with higher scanning speed show the value was 0.428 m^2/g. The maximum adsorption capacity of the adsorbent with a higher surface area at room temperature was 5.42 mg/g.

The fishing net obtained from the household was tested as an adsorbent for gold recovery. FTIR spectrum revealed that material composition was similar to one of nylon-6,6. Adsorption of gold ions on the fishing net was performed at room temperature and 99.23 % of metal removal was achieved. Therefore, fishing nets may be recycled to produce polymer filaments for material extrusion machine where polyamide adsorbent for gold recovery can be manufactured.

SEM pictures of nylon-12 adsorbents both virgin powder and additively manufactured, revealed the presence of gold particles on the surface. Metallic gold observed on the surface of nylon-12 after the adsorption process at different conditions was different in shape and size. Thus, it may be suggested, that adsorption temperature along with adsorption time

influenced the size of gold particles. The optical properties of gold nanoparticles vary based on their size. Hence, AM objects after adsorption at different contact times and different temperatures changed the color from yellow to orange and purple.

According to FTIR spectra and XPS results adsorption mechanism of Au(III) on nylon-12 polymer was proposed. Deconvolution of Au4f gold peak at high-resolution XPS spectrum indicated that the majority of the gold presented on the surface of the polymer is in the state of Au(I). Only a few amounts of gold were adsorbed as Au(III) ions and some amount of gold was reduced to Au(0). Therefore, it was suggested that at first $[AuCl_4]^-$ was attracted electrostatically to protonated amino groups located in amide linkage of nylon-12. After that reduction reaction occurred and Au(III) was reduced to both Au(I) and Au(0) forms. It may be suggested that Au(I) was involved in the formation of the metal complex with nitrogen in the amine groups of the polyamide.

9. SUGGESTIONS FOR FUTURE RESEARCH

For future studies, several aspects can be considered. At first, the desorption process should be studied and based on the obtained knowledge about the chemical state of gold on the nylon-12 surface applicable desorption environment should be suggested. Since Au(I) complex is more stable, it could be tricky to proceed desorption and to recover Au(I) from polymer surface especially when some amount of gold reduced to elemental gold. One may suggest studying the agents that can be added either during adsorption or after adsorption hence to block the transition between complexes of Au. Therefore, if the gold presents on the N12 surface in the form of Au(III) it is more possible to desorb it from the adsorbent surface.

Adsorption efficiency may be increased by modifying the surface of the adsorbent by introducing more active sites. There are several ways how modification can be performed: during the synthesis of the polymer before the AM process, during the AM process by mixing nylon-12 polymer powder with additives and finally, after AM by coating final objects.

Regarding the additive manufacturing aspect, improvements in adsorbent design may be performed to obtain a higher surface area. Conversion of the fishing net into building material for AM should be also studied. Other possibilities of using recycled polymers may be investigated.

REFFERENCES

3DEXPERIENCE Marketplace, 2018. *Introduction to 3D printing - additive processes.* [Online]
Available at: https://make.3dexperience.3ds.com/processes/photopolymerization [Accessed 25 1 2020].

Antler, M., 1983. Gold in electronic components. *Gold Bulletin,* 16(1), pp. 2-7.

Ayawei, N., Ebelegi, A. & Wankasi, D., 2017. Modelling and Interpretation of Adsorption Isotherms. *Journal of Chemistry,* pp. 1-11.

Beard, M., Ghita, O. & Evans, K., 2011. Monitoring the Effects of Selective Laser Sintering (SLS) Build Parameters on Polyamide Using Near Infrared Spectroscopy. *Journal of Applied Polymer Science,* Volume 121, pp. 3153-3158.

Bikas, H., Stavropoulos, P. & Chryssolouris, G., 2016. Additive manufacturing methods and modelling approaches: a critical review. *The International Journal of Advanced Manufacturing Technology,* pp. 389-405.

Blázquez, G., Martín-Lara, M. A., Tenorio, G. & Calero, M., 2011. Batch biosorption of lead(II) from aqueous solutions by olive tree pruning waste:Equilibrium, kinetics and thermodynamic study. *Chemical Engineering Journal,* Volume 168, pp. 170-177.

Bond, G. C., Louis, C. & Thompson, D., 2006. *Catalysis by Gold.* London: Imperial College Press.

Bos, F., Wolfs, R., Ahmed, Z. & Salet, T., 2016. Additive manufacturing of concrete in construction: potentials and challenges of 3D concrete printing. *Virtual and Physical Prototyping.*

Brydson, J. A., 1999. Polyamides and Polyimides. In: *Plastics Materials* . Oxford : Butterworth-Heinemann, pp. 478-529.

Buchtenirch, M., 2004. *Gold colored alloy used for dentistry and jewelry.* United States, Patent No. US6835252B1.

Caulfield, B., McHugh, P. & Lohfeld, S., 2007. Dependence of mechanical properties of polyamide components on build parameters in the SLS process. *Journal of Materials Processing Technology,* Volume 182, pp. 477-488.

Chan, H. S. O. et al., 1990. GX-Ray Photoelectron Spectroscopic Studies of Polyquinazolones: An Assessment of the Degree of Cyclization. *Polymer Journal,* Volume 22, pp. 883-892.

Chiou, C., 2002. Fundamentals of the Adsorption Theory. In: *Partition and Adsorption of Organic Contaminants in Environmental Systems.* s.l.:John Wiley & Sons, Inc., p. 39.

Clarkson, R., 1997. *A2 Inorganic Chemistry - Electrode Potentials and Transition Metals.* [Online]
Available at: http://www.chemistryrules.me.uk/tandp/optiontransitionelements.htm [Accessed 3 1 2019].

Coates, J., 2006. Interpretation of Infrared Spectra, A Practical Approach. In: *Encyclopedia of Analytical Chemistry.* s.l.:s.n., pp. 1-23.

Craft, G. M., 2018. *Characterization of Nylon-12 in a Novel Additive Manufacturing Technology, and the Rheological and Spectroscopic Analysis of PEG-Starch Matrix Interactions.* [Online]
Available at: https://scholarcommons.usf.edu/etd/7137/ [Accessed 9 January 2020].

Cytodiagnostic Inc., 2017. *Gold Nanoparticle Properties.* [Online]
Available at: http://www.cytodiagnostics.com/store/pc/viewcontent.asp?idpage=2 [Accessed 30 January 2020].

Das, M., Shim, K. H., An, S. S. A. & Yi, D., 2011. Review on gold nanoparticles and their applications. *Toxicology and Environmental Health Sciences,* 3(4), pp. 193-205.

Das, M., Shim, K. H., An, S. S. A. & Yi, D. K., 2011. Review on Gold Nanoparticles and Their Applications. *Toxicol. Environ. Health. Sci.,* 3(4), pp. 193-205.

Deckers, J., Vleugels, J. & J-P, K., 2014. Additive Manufacturing of Ceramics: A Review. *Journal of Ceramic Science and Technology,* pp. 245-260.

Deng, S., Bai, R. & Chen, J., 2003. Aminated Polyacrylonitrile Fibers for Lead and Copper Removal. *Langmuir,* Volume 19, pp. 5058-5064.

Dokoutchaev, A. et al., 1999. Colloidal metal deposition onto functionalized polystyrene microsphere. *Chemistry of Materials,* Volume 11, pp. 2389-2399.

Duddleston, L., Harris, A., Puck, A. T. & Doll, N., 2016. *Polyamide (Nylon) 12 Degradation during the Selective Laser Sintering (SLS) Process: A Quantification for Recycling Optimization.* Indianapolis, ANTEC 2016.

Đurovic´, M. D., Bugarc˘ic´, Z. D. & Eldik, R., 2017. Stability and reactivity of gold compounds – From fundamental aspects to applications. *Coordination Chemistry Reviews,* Volume 338, pp. 186-206.

El-Khaiary, M., 2008. Least-squares regression of adsorption equilibrium data: Comparing the options. *Journal of Hazardous Materials,* 158(1), pp. 73-87.

Engineering product design, 2017. *Material Extrusion.* [Online] Available at: https://engineeringproductdesign.com/knowledge-base/material-extrusion/ [Accessed 25 1 2020].

EOS GmbH - Electro Optical System, 2017. *Product Information.* [Online] Available at: https://materflow.com/wp-content/uploads/2018/07/material-data-pa2200.pdf [Accessed 10 10 2019].

Faraday, M., 1857. Experimental relations of gold (and other metals) to light. *Philosophical Transactions of the Royal Society of London,* Volume 147, pp. 145-181.

Feng, B. et al., 2018. Highly efficient and selective recovery of Au(III) from a complex system by molybdenum disulfide nanoflakes. *Chemical Engineering Journal,* Volume 350, pp. 692-702.

Feng, L., Wang, Y. & Wei, Q., 2019. PA12 Powder Recycled from SLS for FDM. *Polymers,* Volume 11, pp. 1-12.

Fierro, V., Torne´-Ferna´ndez, V., Montane´, D. & Celzard, A., 2008. Adsorption of phenol onto activated carbons having different textural and surface properties. *Microporous and Mesoporous Materials ,* Volume 111, p. 276–284.

Flodberg, G., Pettersson, H. & Yang, L., 2018. Pore analysis and mechanical performance of selective laser sintered objects. *Additive Manufacturing,* Volume 24, pp. 307-315.

Fornalczyk, A., Willner, J., Francuz, K. & Cebulski, J., 2013. E-waste as a source of valuable metals. *Archives of Materials Science and Engineering ,* 63(2), pp. 87-92.

Gibson, I., Rosen, D. & Stucker, B., 2015. Introduction and Basic Principles. In: *Additive Manufacturing Technologies.* New York: Springer-Verlag New York, pp. 1-10.

Gimeno, M. C., 2008. The Chemistry of Gold. In: A. Laguna, ed. *Modern Supramolecular Gold Chemistry: Gold-Metal Interactions and Applications.* Weinheim: WILEY-VCH Verlag GmbH & Co. KGaA, pp. 1-64.

Griehl, W. & Ruestem, D., 1970. Nylon-12 - Preparation, properties and applications. *Industrial and Engineering Chemistry ,* 62(3), pp. 16-22.

Gulnaz, O., Saygideger, S. & Kusvuran, E., 2005. Study of Cu(II) biosorption by dried activated sludge: effect of physico-chemical environment and kinetics study. *Journal of Hazardous Materials,* Volume 120, pp. 193-200.

Gurung, M. et al., 2011. Quaternary Amine Modified Persimmon Tannin Gel: An Efficient Adsorbent for the Recovery of Precious Metals from Hydrochloric Acid Media. *Separation Science and Technology ,* 46(4), pp. 2250-2259.

Han, J., Cao, Z. & Gao, W., 2013. Remarkable sorption properties of polyamide 12 microspheres for a broad-spectrum antibacterial (triclosan) in water. *Journal of Materials Chemistry,* Volume 1, p. 4941–4944.

Hofland, E., Baran, I. & Wismeijer, D., 2017. Correlation of Process Parameters with Mechanical Properties of Laser Sintered PA12 Parts. *Advances in Materials Science and Engineering,* pp. 1-11.

Ho, H., Gibson, I. & Cheung, W., 1999. Effects of Energy Density on Morphology and Properties of Selective Laser Sintered Polycarbonate. *Journal of Materials Processing Technology,* Volume 89-90, pp. 204-210.

Hokkanen, A. et al., 2017. Comparison of adsorption equilibrium models and error functions for the study of sulfate removal by calcium hydroxyapatite microfibrillated cellulose composite. *Environmental Technology.*

Housecroft, C. E. & Sharpe, A. G., 2001. d-Block chemistry: coordination complexes. In: *Inorganic Chemistry.* London: Pearson Education Limited, pp. 555-592.

Huang, P. T., Kwei, T. K., Pearce, E. M. & V, L. S., 2001. Blends of nylon-6 with phenol-containing polymers. *Polymer Chemistry,* 39(6), pp. 841-850.

Innocentini, M. et al., 2019. Lattice-shaped geopolymer catalyst for biodiesel synthesis fabricated by additive manufacturing. *Ceramics International,* 45(1), pp. 1443-1446.

Javaid, M. & Haleem, A., 2019. 3D printed tissue and organ using additive manufacturing: An overview. *Clinical Epidemiology and Global Health.*

Jermakowicz-Bartkowiak, D., Kolarz, B. N. & W*l*odzimierz, T., 2003. Sorption of aurocyanide and tetrachloroaurate onto resin with guanidine ligand—an XPS approach. *Polymer,* Volume 44, p. 5797–5802.

Jung, M. R. et al., 2018. Validation of ATR FT-IR to identify polymers of plastic marine debris, including those ingested by marine organisms. *Marine Pollution Bulletin,* Volume 127, pp. 704-716.

Kecili, R. & Hussain, C. M., 2018. Mechanism of Adsorption on Nanomaterials . In: *Current Trends in Chromatographic Research Technology and Techniques.* s.l.:Elsevier , pp. 89-115.

Kerber, S. J. et al., 1996. The nature of hydrogen in x-ray photoelectron spectroscopy:General patterns from hydroxides to hydrogen bonding. *Journal of Vacuum Science & Technology A,* Volume 14, pp. 1314-1320.

Kim, B. C., 2000. Modification of Nylon. In: J. J. Meister, ed. *Polymer Modification. Principles, Techniques, and Applications.* New York: Marcel Dekker, Inc., pp. 433-473.

Kiraz, C., Sezer, K. & şahin, I., 2018. A perspective on exploiting the design freedom of 3D printers in jewellery industry. *International Journal of 3D Printing Technologies and Digital Industry,* Volume 2, pp. 46-58.

Kumar, L. J. & Nair, C. G. K., 2017. Current Trends of Additive Manufacturing in the Aerospace Industry. *Advances in 3D Printing & Additive Manufacturing Technologies.*

Kyulavska, M., Toncheva-Moncheva, N. & Rydz, J., 2019. Biobased Polyamide Ecomaterials and Their Susceptibility to Biodegradation. In: *Handbook of Ecomaterials.* Switzerland: Springer Nature Switzerland, pp. 2901-2927.

Lagergren, S., 1898. About the Theory of So-Called Adsorption of Soluble Substances. *Kungliga Svenska Vetenskapsakademien,* Volume 24, pp. 1-39.

LCGC's CHROM academy, 2014. *Introduction to IR Spectroscopy.* [Online] Available at: https://www.chromacademy.com/lms/sco533/01-infrared-spectroscopy-introduction.html?fChannel=14&fCourse=77&fSco=533&fPath=sco533/01-infrared-spectroscopy-introduction.html

[Accessed 13 10 2019].

Limousin, G. et al., 2007. Sorption isotherms: A review on physical bases, modeling and measurement. *Applied Geochemistry,* 22(2), pp. 249-275.

Lipton, J. I. et al., 2015. Additive manufacturing for the food industry. *Trends in Food Science & Technology,* 43(1), pp. 114-123.

Liu, L., Luo, X.-B., Ding, L. & Luo, S.-L., 2019. 4 - Application of Nanotechnology in the Removal of Heavy Metal From Water. In: *Nanomaterials for the Removal of Pollutants and Resource Reutilization.* s.l.:Elsevier Inc., pp. 89-90.

Liu, Y., 2008. New insights into pseudo-second-order kinetic equation for adsorption. *Colloids and Surfaces A: Physicochemical and Engineering Aspects,* 320(1-3), pp. 275-278.

Li, X. et al., 2013. Efficient adsorption of gold ions from aqueous systems with thioamide-group chelating nanofiber membranes. *Chemical Engineering Journal,* Volume 229, pp. 420-428.

Lodhi, M., Deen, K. & Haider, W., 2019. Additively manufactured 316L stainless steel: An efficient electrocatalyst. *International Journal of Hydrogen Energy,* 44(45), pp. 24698-24704.

Manoharan, S. et al., 2019. Comparing the Economics of Metal Additive Manufacturing Processes for Micro-scale Plate Reactors in the Chemical Process Industry. *Procedia Manufacturing,* Volume 34, pp. 603-612.

Matsuda, M. et al., 1979. Recovery of gold from the plating rinse by adsorption with nylon fibers. *Desalination ,* Volume 29, pp. 275-284.

Mihăilescu, M. et al., 2019. Gold (III) adsorption from dilute waste solution onto Amberlite XAD7 resin modified with L-glutamic acid. *Schientific reports,* 9(8757).

Mironov, I. V. & Makotchenko, E. V., 2009. The Hydrolysis of AuCl4 and the Stability of Aquachlorohydroxocomplexes of Gold(III) in Aqueous Solution. *J Solution Chem,* Volume 38, pp. 725-737.

Miyanaji, H. et al., 2016. Process development of porcelain ceramic material with binder jetting process for dental applications. *The Journal of The Minerals, Metals & Materials Society (TMS) ,* 68(3), pp. 831-841.

Ngo, T. D. et al., 2018. Additive manufacturing (3D printing): A review of materials, methods,applications and challenges. *Composites Part B,* pp. 172-196.

Ngo, T. D. et al., 2018. Additive manufacturing (3D printing): A review of materials, methods, applications and challenges. *Composites Part B,* Volume 143, pp. 172-196.

Novak, I., Steviar, M. & Chodak, I., 2006. Surface Energy and Adhesive Properties of Polyamide 12 Modified by Barrier and Radio-Frequency Discharge Plasma. *Monatshefte fuer Chemie/Chemical Monthly,* Volume 137, pp. 943-952.

Ogata, T. & Nakano, Y., 2005. Mechanisms of gold recovery from aqueous solutions using a novel tannin gel adsorbent synthesized from natural condensed tannin. *Water Research,* 39(18), pp. 4281-4286.

Panyala, N. R., Peña-Méndez, E. & Havel, J., 2009. Gold and nano-gold in medicine: overview, toxicology and perspectives. *Journal of Applied Biomedicine,* Volume 7, pp. 75-91.

Park, S.-J. & Seo, M.-K., 2011. Element and Processing. In: *Interface Science and Composites.* s.l.:Elsevier Ltd. , pp. 431-499.

Pearson, R. G., 1963. Hard and soft acids and basis. *Journal of the American Chemical Society,* Volume 85, pp. 3533-3539.

Pluchery, O., Remita, H. & Schaming, D., 2013. Demonstrative experiments about gold nanoparticles and nanofilms: an introduction to nanoscience. *Gold Bull,* Volume 46, pp. 319-327.

Rapidsol. 3D Printing Service , 2015. *Blog.* [Online] Available at: https://www.rapidsol.org/blogitem.aspx?id=10 [Accessed 25 1 2020].

Redwood, B., Schöffer, F. & Garret, B., 2017. *The 3D Printing Handbook.* Amsterdam: 3D Hubs B.V..

Repo, E., 2011. *EDTA- and DTPA-functionalized silica gel and chitosan adsorbents for the removal of heavy metals from aqueous solutions,* s.l.: LUT-yliopisto.

Rouquerol, F. et al., 2014. Introduction. In: *Adsorption by Powders and Porous Solids.* Amsterdam: Elsevier Ltd., pp. 1-21.

Rubcumintara, T., 2015. Adsorptive Recovery of Au(III) from Aqueous Solution Using Modified Bagasse Biosorbent. *International Journal of Chemical Engineering and Applications,* 6(2), pp. 95-100.

Sciencenter, 2011. *Exploring Materials—Nano Gold.* [Online] Available at: https://www.nisenet.org/sites/default/files/catalog/uploads/8880/materialsgold_guide_31oct11.pdf [Accessed 28 January 2020].

Scott, A. F., 1973. *Survey of Progress in Chemistry.* London: Academic Press .

Shibata, J. & Okuda, A., 2002. Recycling technology of precious metals. *Journal of the Mining and Materials Processing Institute of Japan,* Volume 118, pp. 1-8.

Smith, B., 1999. *Infrared spectral interpretation : a systematic approach.* Boca Raton : CRC Press LLC.

Thompson, D., 2007. Michael Faraday's Recognition of Ruby Gold: the Birth of Modern Nanotechnology. *Gold Bulletin,* 40(4), pp. 267-269.

Tsai, S.-W.et al., 2019. Additive Manufacturing of Electrodes for Desalination. *Procedia Manufacturing,* Volume 34, pp. 252-259.

Uehara, A., Chang, S., Booth, S. G. & Schroeder, S. L. M., 2016. Redox and Ligand Exchange during the Reaction of Tetrachloroaurate with Hexacyanoferrate(II) at a Liquid-Liquid Interface: Voltammetry and X-ray Absorption Fine-Structure Studies. *Electrochimica Acta,* Volume 190, pp. 997-1006.

van de Werken, N. et al., 2020. Additively manufactured carbon fiber-reinforced composites: State of the art and perspective. *Additive Manufacturing,* Volume 31.

Wang, T., Tan, Q., Chiang, J. & Li, J., 2017. Recovery of rare and precious metals from urban mines—A review. *Frontiers of Environmental Science & Engineering,* Volume 11, pp. 1-17.

Weijmarshausen, P., 2014. *3D Print in Nylon with Selective Laser Sintering – Part 3.* [Online]
Available at: https://www.shapeways.com/blog/archives/17704-3d-print-in-nylon-with-selective-laser-sintering-part-3.html
[Accessed 13 10 2019].

Wen, F. et al., 2008. Synthesis of noble metal nanoparticles embedded in the shell layer of core-shell poly(styrene-co-4-vinylpyridine) micospheres and their application in catalysis. *Chemistry of Materials,* Volume 20, pp. 2144-2150.

Wu, F.-C., Tseng, R.-L. & Juang, R.-S., 2009. Characteristics of Elovich equation used for the analysis of adsorption kineticsin dye-chitosan systems. *Chemical Engineering Journal,* Volume 150, pp. 366-373.

Wu, F.-C., Tseng, R.-L. & S., J. R., 1999. Role of pH in metal adsorption from aqueous solutions containing chelating agents on chitosan. *Industrial & Engineering Chemistry Research,* pp. 270-275.

Xu, J. B., Zhao, T. & Liang, Z., 2008. Carbon supported platinum–gold alloy catalyst for direct formic acid fuel cells. *Journal of Power Sources,* 185(0), pp. 857-861.

Yi, L., Gläßner, C. & Aurich, J. C., 2019. How to integrate additive manufacturing technologies into manufacturing systems successfully: A perspective from the commercial vehicle industry. *Journal of Manufacturing Systems,* Volume 53, pp. 195-211.

Zadpoor, A. A. & Malda, J., 2017. Additive Manufacturing of Biomaterials, Tissues, and Organs.. *Annals of Biomedical Engineering.*

Zhang, H., Ritchie, I. M. & La Brooy, S. R., 2004. The adsorption of gold thiourea complex onto activated carbon. *Hydrometallurgy ,* Volume 72, pp. 291-301.

Zhang, R.-C.et al., 2017. Gold nanoparticle-polymer nanocomposites synthesized by room temperature atmospheric pressure plasma and their potential for fuel cell electrocatalytic application. *Scientific Reports,* pp. 1-9.

Zhao, J. et al., 2019. Selective recovery of Au(III) from wastewater by a recyclable magnetic Ni0.6Fe2.4O4 nanoparticels with mercaptothiadiazole: Interaction models and adsorption mechanisms. *Journal of Cleaner Production,* Volume 236, pp. 1-13.

Zorn, G. et al., 2014. X-Ray Photoelectron Spectroscopy Investigation of the Nitrogen Species in Photoactive Perfluorophenylazide-Modified Surfaces. *The Journal of Physical Chemistry. C, Nanomaterials Interfaces,* Volume 118, p. 376–383.